Simulations with exact and chirally improved fermions

K. Jansen

John von Neumann-Institute for Computing, DESY, Platanenallee 6, D-15738 Zeuthen, Germany

Abstract

We review simulations of lattice of QCD with chiral invariant overlap fermions and chirally improved maximally twisted mass fermions. We discuss simulations with twisted mass fermions for $N_f = 2$ flavours of mass degenerate quarks and for the situation of $N_f = 2 + 1 + 1$ flavours, where the strange and the charm quarks are taken into account as active degrees of freedom. Results are presented for a number of physical quantities among which are the muon anomalous magnetic moment, pseudo scalar masses and decay constants, quark masses, the pion scattering length and the ρ-meson resonance. In addition, we discuss aspects of the simulations themselves and the non-perturbative renormalization that has been performed. Finally, first result are given for simulations directly at the physical value of the pion mass.

Keywords: Lattice QCD, simulations, muon anomalous magnetic moment, scattering amplitudes, renormalization, decay constants

1. Introduction

In this contribution to the proceedings of the Transregional Collaborative Research Center 9 "Computational Particle Physics" we report on an effort to develop and test new formulations of lattice QCD and new algorithms. In particular, the goal of this work has been to develop a lattice fermion formulation and an algorithm that allows for computations as close as possible to the physical value of the pion mass. At the same time, the lattice theory should possess an improved (if not exact) chiral symmetry. In addition, the derived lattice theory should be such that all physical quantities have lattice artefacts that appear only at $O(a^2)$ thus avoiding linear discretization effects as they appear for, e.g., standard Wilson fermions.

Table 1 shows that this goal could be reached even more than has been anticipated. In the table, we show ratios of meson masses and meson decay constants that *were obtained directly at the physical value of the pion mass,* see also ref. [1, 2]. The lattice results are compared to the corresponding data from the particle data group (PDG) [3] and we find a nice agreement demon-

strating that we indeed have reached the physical value of the pion mass and that lattice QCD reproduces the measured meson masses and decay constants.

In fig. 1 we show, as an important quantity to detect physics beyond the standard model, the leading order hadronic light quark contribution to the muon anomalous magnetic moment [4]. Here, lattice results are shown that were obtained at unphysical values of the pion mass and which needed to be extrapolated to the physical pion mass. In addition, we show the results from a direct calculation at the physical point. In this case, the chiral extrapolation nicely agrees with the direct computation. For other quantities, such as the nucleon axial charge or the average momentum of a quark in a nucleon, only the physical point calculations tend to their experimental or phenomenologically determined values, see [5].

In the following sections we want to illustrate, how it became possible to perform at the end of this transregional collaborative research center simulations directly at the physical point.

The outline of this contribution is as follows. In sec-

	M_{Ds}/M_K	M_{Ds}/M_D	f_K/f_π	f_{Ds}/f_D
lat.	3.96(2)	1.049(4)	1.197(6)	1.19(2)
PDG	3.988	1.0556(02)	1.197(06)	1.26(6)

Table 1: Comparison of ratios of meson masses and decay constants obtained from our first computations at the physical point with the corresponding values taken from the PDG.

tion 2 we discuss the starting point of this project, the exploration of lattice fermions [6, 7] that respect an exact, lattice modified chiral symmetry [8]. Although these kind of lattice fermions are conceptually very advantageous, it turned out that they are computationally very expensive, in fact, so expensive that presently they almost cannot be used for dynamical fermion simulations [9, 10]. We therefore switched to so-called twisted mass fermions [11, 12] which are explained in section 3. Section 4 is devoted to our first simulations with twisted mass simulations with $N_f = 2$ flavours of mass-degenerate light quarks. In section 5, we discuss some highlights from the simulations, scattering amplitudes and the muon anomalous magnetic moment. Our efforts to carry through a non-perturbative renormalization is outlined in section 6 and section 7 describes the extension of the simulations including the complete first two quark generations as active degrees of freedom. Section 8 has further selected results and we conclude in section 9, where we also give an outlook.
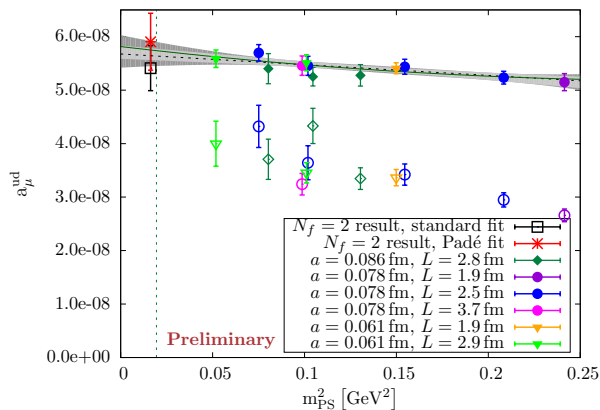

Figure 1: In the graph, we show the light quark contribution to the leading order hadronic contribution to the muon anomalous magnetic moment. The set of open and filled symbols represent two different lattice definitions of the muon anomalous magnetic moment, as will be discussed in more detail in section 5.

2. Chiral invariant and chirally improved lattice fermions

When K. Wilson proposed his formulation of QCD on a Euclidean space-time lattice [13], he had to compromise between the appearance of unwanted doubler modes and a breaking of chiral symmetry on a lattice since both properties cannot be maintained at the same time. In particular, Wilson's lattice Dirac operator reads

$$\hat{D}_{\text{Wilson}}(m_q) = \frac{1}{2}\left(\gamma_\mu(\nabla_\mu^* + \nabla_\mu) - r\nabla_\mu^*\nabla_\mu\right) + m_q, \quad (1)$$

where ∇_μ (∇_μ^*) denotes the forward (backward) lattice derivative, m_q is the bare quark mass and r the Wilson parameter. The second order derivative term $r\nabla_\mu^*\nabla_\mu$ lifts –on the one hand– the doubler modes which receive a mass proportional to r/a such that in the limit of vanishing lattice spacing a they become infinitely heavy and decouple. On the other hand, since this term acts like a mass term, chiral symmetry is explicitly broken even for mass-less quarks at $m_q = 0$. Chiral symmetry is the invariance of the action S_{latt} under the interchange of mass-less left-handed and right-handed quarks which can be mathematically expressed by the anti-commutation relation $\{\gamma_5, D_{\text{latt}}\} = 0$.

The clash between a lattice formulation of the quark and gluon interaction and chiral symmetry has then been formalized in the infamous Nielsen-Ninomiya theorem [14, 15, 16]. It states that a theory that shows point-like localization, has the property of chiral symmetry, describes only one quark species and converges to the correct continuum quark propagator cannot be consistently formulated on a space-time lattice.

Although in a seminal work [17] it could be demonstrated that to all orders of perturbation theory chiral symmetry in Wilson's formulation of lattice gauge theory will be recovered in the continuum limit, the search for an exactly chirally invariant lattice formulation had been actively pursued in the lattice community. One reason has been that the breaking of chiral symmetry leads to unwanted effects such as the necessity of additive mass renormalization or the apparent impossibility to formulate a chiral gauge theory on the lattice.

A solution to this problem was provided by the Ginsparg-Wilson relation [18],

$$\gamma_5 D_{\text{latt}} + D_{\text{latt}}\gamma_5 = a D_{\text{latt}}\gamma_5 D_{\text{latt}} \quad (2)$$

which states that the anti-commutation relation of the Dirac operator and γ_5 is not zero as in the continuum but allows for a right hand side which is, however, multiplied with the lattice spacing. In this way, at vanishing

lattice spacing the continuum chiral symmetry relation is restored.

The full power of the Ginsparg-Wilson relation showed up, when it was realized [8] that any lattice Dirac-operator which fulfills this relation implies an exact lattice chiral symmetry

$$\Psi \rightarrow \gamma_5 \left(1 - \frac{a}{2} D_{\text{latt}}\right) \Psi \, , \bar{\Psi} \rightarrow \bar{\Psi} \left(1 - \frac{a}{2} D_{\text{latt}} \gamma_5\right) . \quad (3)$$

Consequences from this observation are far reaching [19]: the index theorem can be established on the lattice, many renormalizations become trivial or mixing patterns in the renormalization can be avoided. The Ginsparg-Wilson (GW) relation laid therefore a solid theoretical ground for a chiral invariant lattice theory of quantum chromodynamics. At the time the GW relation was derived, no practical solution could be found that could be used in numerical simulations. It is remarkable that only 17 years later the importance of the GW relation was rediscovered [20] and candidate lattice Dirac operators were proposed [21]. A concrete realization for an operator that satisfies the GW relation has been suggested in [6, 7] in form of the so-called overlap operator,

$$\hat{D}_{\text{overlap}}(0) = \frac{1}{a}\left(1 - A(A^\dagger A)^{-1/2}\right). \quad (4)$$

The kernel operator A reads:

$$A = 1 + s - a\hat{D}_{\text{Wilson}}(0), \quad (5)$$

where D_{Wilson} is the Wilson-Dirac operator of eq. (1), s is a parameter which satisfies $|s| < 1$. This overlap operator could be shown to be local [22] in the sense that it is exponentially bounded and the parameter s can be used to optimize the locality properties of $\hat{D}_{\text{overlap}}(0)$. A quark mass can be added to the overlap operator in a rather straightforward way,

$$\hat{D}_{\text{overlap}}(m_{\text{ov}}) = \left(1 + s - \frac{a m_{\text{ov}}}{2}\right)\hat{D}_{\text{overlap}}(0) + m_{\text{ov}}, \quad (6)$$

where m_{ov} is the bare overlap quark mass.

The above sketched overlap operator has been in the focus of the first period of this project. An important goal has been to find efficient ways to evaluate $\hat{D}_{\text{overlap}}$ numerically. In [9, 10] a very comprehensive test of various algorithmic methods has been performed which allowed to identify the optimal way to carry out computations with the overlap operator. It needs to be stressed, though, that all numerical computations with the overlap operator have been performed in the quenched approximation where the fermion determinant is set to one. Thus, internal sea quark loops have been neglected.

In this quenched approximation, it became possible to employ the overlap operator for calculations in the ϵ-regime of chiral perturbation theory [23, 24, 25] to analyze the low-lying eigenvalue spectrum [26] and various meson correlation functions [27]. As a result, a number of low energy constants of chiral perturbation theory could be determined. We show in fig. 2, as an example the comparison of the cumulative eigenvalue distribution as computed numerically using the overlap operator and the analytical prediction from random matrix theory [28, 29, 30, 31]. From this comparison a value of the chiral condensate of $\Sigma \approx (253\text{MeV})^3$ could be extracted which is in a good agreement with other determinations performed at that time in the quenched approximation.
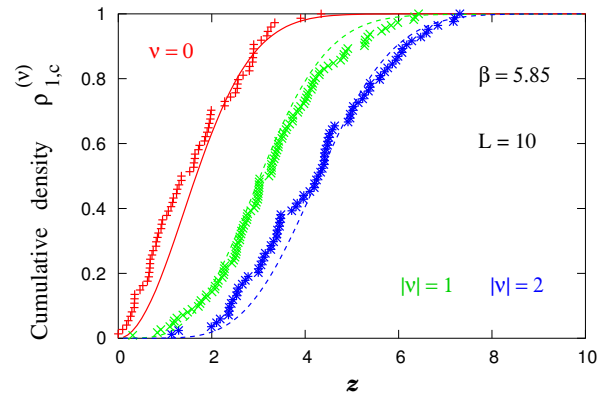

Figure 2: The cumulative distribution of the lowest non-zero eigenvalue on a 10^4 lattice for a lattice spacing of $a \approx 0.1\text{fm}$. We show the random matrix theory (RMT) predictions (lines) and results for topological charges $|\nu| = 0, 1, 2$. We find a satisfactory agreement with RMT, if the chiral condensate is chosen optimally. This requires $\Sigma \approx (253\text{MeV})^3$.

For the quenched investigation of the ϵ-regime, small volumes such as $16^3 32$ are often sufficient for which the overlap operator can be evaluated with an acceptable computational cost. However, when larger volumes are needed, it turned out that the cost for using the overlap operator exceeds a factor of hundred when compared to Wilson like fermions, [9, 10]. Moreover, employing the overlap operator for dynamical fermions, also a conceptual problem appears since the overlap operator has exact, topological zero modes [32]. This led to a general skepticism in the lattice community that dynamical overlap simulations will become practical for large volumes, a skepticism that in fact turned out to be true.

Note, however, that through a number of special algorithmic tricks [33] the overlap operator has been used very successfully for analyzing a Higgs-Yukawa model on the lattice [34]. In these works, the phase structure

of the model [35, 36], lower and upper Higgs boson mass bounds [37, 38], Higgs boson resonance parameters [39] and the influence of heavier quarks [40, 41] and higher dimensional operators [42] have been worked out.

3. Twisted mass fermions

The very large computational cost of overlap fermions made it necessary to look for alternative formulations of lattice QCD which should owe the properties outlined in the introduction. In ref. [11] a proposal for lattice fermions appeared in form of twisted mass fermions which could later be shown to lead to an automatic O(a)-improvement [12], as will be discussed below.

Twisted mass fermions are a variant of Wilson fermions with a (2-flavour) Dirac operator of the form

$$\hat{D}_{\text{TM}} = \hat{D}_{\text{Wilson}}(m_q) + i\mu_q\gamma_5\tau_3, \qquad (7)$$

where μ_q is an additional mass parameter, called the twisted mass and τ_3 is the third Pauli matrix acting in flavour space.

This twisted mass formulation of lattice QCD promised to realize an automatic $O(a)$ improvement such that all physical quantities scale with a rate of $O(a^2)$ towards the continuum limit. What made this approach very attractive is that the automatic $O(a)$-improvement [12] is based on symmetry arguments alone, thus providing a clean and solid theoretical ground. It goes beyond the scope of this article to provide the arguments that lead to automatic $O(a)$-improvement and we refer to ref. [43] for a review on the subject. Twisted mass fermions also lead to a regularization of small, unphysical eigenvalues that appear in other Wilson-type formulations of lattice QCD, a property that makes twisted mass fermions very attractive for numerical simulations, and the maximally twisted mass setup simplifies certain renormalization procedures.

The paper [12] has been a turning point of this work. We decided to test this promising approach to lattice QCD, first in the quenched approximation. In particular, in ref. [44] we could demonstrate that twisted mass fermions at maximal twist indeed allows to reach very small pion masses, much below what has been possible with standard or improved Wilson fermions. In a detailed lattice spacing scaling test [45, 46, 47] it became also possible to demonstrate the anticipated automatic $O(a)$ improvement of maximally twisted mass fermions, see fig. 3.

In the course of this scaling test, an optimal way for tuning to maximal twist could be established. While in our first attempt we aimed at setting the pion mass to zero, it turns out that a much better way is to tune the bare Wilson quark mass m_q such that the PCAC quark mass,

$$m_{\text{PCAC}} = \frac{\sum_{\mathbf{x}}\langle\partial_0 A_0^a(x)P^a(0)\rangle}{2\sum_{\mathbf{x}}\langle P^a(x)P^a(0)\rangle}, \qquad a = 1, 2 \qquad (8)$$

vanishes. This corresponds to tuning the theory to a critical value of the quark mass, $m_{q,\text{crit}}$ or to a critical value of the hopping parameter κ, $\kappa_{\text{crit}} = 1/(8+2am_{q,\text{crit}})$. Note that the PCAC quark mass is optimally evaluated at large enough time separation, such that the pion ground state is dominant.

Employing this definition of maximal twist not only the nice scaling behaviour in the square of the lattice spacing as shown in fig. 3 could be established, but it could also be demonstrated that the remaining $O(a^2)$ effects are small. We anticipate already here that this very good lattice scaling behaviour was also found in a later stage of this work when the quenched approximation could be overcome and the quarks acted as truly active degrees of freedom in the simulations [48, 49, 50, 51]. These findings are in full agreement with the theoretical analysis performed in ref. [52] which also suggests to tune the PCAC quark to zero to realize maximal twist in an optimal way.
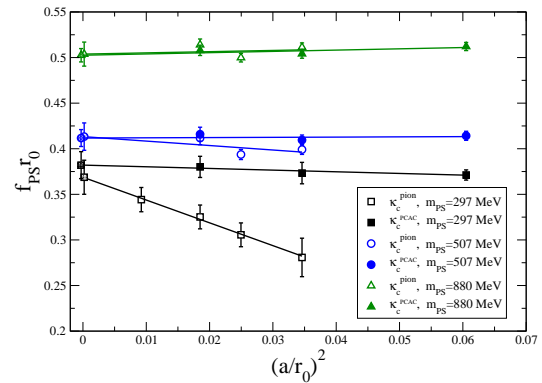

Figure 3: The continuum limit scaling behaviour of the pion decay constant. We show results for maximally twisted mass fermions for two definitions to realize maximal twist.

The major drawback of twisted mass fermions is the fact that they break isospin explicitly resulting in different masses for, e.g. the charged and the neutral pions. This flavour breaking effect has been analyzed in ref. [53] and at least in the quenched approximation a tolerably small flavour breaking effect has been found.

Although the isospin violation is only an $O(a^2)$ lattice artefacts, it can have severe consequences. It influences the phase structure of lattice QCD which can lead to instabilities in the numerical simulations, see below. It also gives rise to additional finite size effects as predicted from chiral perturbation theory [54, 55, 56]. The breaking of isospin has been thoroughly investigated theoretically [57]. The conclusion of this paper has been that only quantities are affected that are related to the neutral pion mass. Nevertheless, this particular lattice artefact needed to and has been monitored in the course of the work employing twisted mass fermions.

3.1. First simulations with active up and down quarks

The success of the quenched computations described above made the twisted mass approach to be a very promising candidate for dynamical lattice QCD simulations. Moreover, as the twisted mass term provides an explicit infra-red regulator for the fermion matrix and avoids thus unwanted unphysical small eigenvalues of the Wilson-Dirac operator, employing twisted mass fermions leads to safe simulations. This fact has been –at least in the beginning– a major motivation for using twisted mass fermions [58]. It was then found later that the effect of the fermion determinant itself can also help substantially to suppress these small eigenvalues [59, 60].

Staying within the setup of twisted mass fermions, first dynamical simulations of twisted mass fermions were started. It is worth emphasizing that we developed different programme codes [61, 61, 62], including even codes for the APE-machines [63]. Since these codes also used different realizations of the standard simulation algorithms, we could therefore cross-check all our numerically obtained results in an independent way.

When starting these first twisted mass numerical simulations, we experienced a surprise. In contrast to our expectation that the simulations should be safe, we found that they are in fact unstable manifesting itself by the appearance of a metastable behaviour [64, 65, 66, 67]. This effect could be demonstrated performing simulations with cold (completely ordered) or hot (completely random) gluon field configurations [64]. The two simulations led to different plaquette values as can be seen in fig. 4.

The behaviour of the simulations could be understood from the results of ref. [68]. In this paper, an analysis of the effective potential within the framework of chiral perturbation theory has been performed for twisted mass fermions. Depending on the parameter values of the action, the bare Wilson and the bare twisted mass parameter, two different scenarios were found in this analysis.
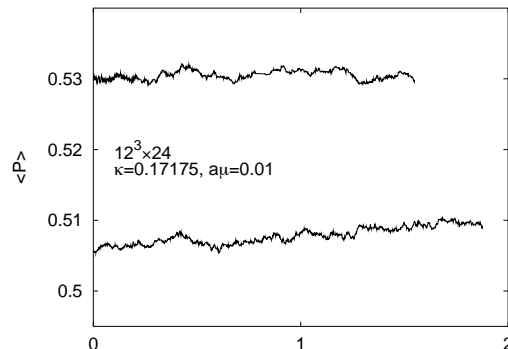

Figure 4: Metastable states. The number of sweeps is given in thousands. The lattice size is $12^3 \times 24$ and the twisted mass is $\mu_q = 0.01$.

The first situation leads to a single minimum of the effective potential while the second situation to a double well effective potential.

These two shapes of the effective potential lead to different phenomena: the first case (single minimum) corresponds to a second order behavior –we speak of an Aoki scenario [69]– while the second case belongs to a first order behaviour –which is referred to as the Sharpe-Singleton scenario. The suspicion that the behaviour of the simulations originates from being in the first order scenario made it necessary to investigate the situation in more detail. To this end, we performed thermal cycles, see fig. 5 and also ref. [66].

It is only possible to establish from numerical simulations the existence of a first order phase transition through a detailed and demanding finite size analysis. Such an analysis is very difficult when quarks are taken as active degrees of freedom in the simulations. However, we found through investigations as described above, very strong evidence that we are indeed in the Sharpe-Singleton scenario. In addition, a number of analytical work was carried out [70, 71, 72, 73, 74, 75, 76, 55] and a full consistency with our numerical simulation results has been found. For an analysis of the Aoki scenario, see ref. [77].

The difficulty with the first order phase transition of the Sharpe-Singleton scenario is that it becomes very difficult, if not impossible, to go to small quark masses since the simulations there the simulations become unstable with not very well defined results due to the first order scenario. Note that this effect is a pure lattice artefact which vanishes towards the continuum limit.

It became therefore necessary to find a lattice action

that avoids the first order behaviour as much as possible to allow for simulations at small quark masses. We carried out therefore a test of various actions [65, 78, 64, 66, 67] with the conclusion that employing an improved gauge action, the tree-level Symanzik action [79, 80], is sufficient to weaken the first order behaviour enough such that safe simulations at pion masses of about 300MeV become possible.

The setup of using the Symanzik improved gauge action and maximally twisted mass fermions for 2 flavours of mass-degenerate quarks has been the starting point for first calculations with active up and down quarks [58]. In this work, we could in fact reach pion masses of about 300MeV which at the time of the publication has been a major achievement.
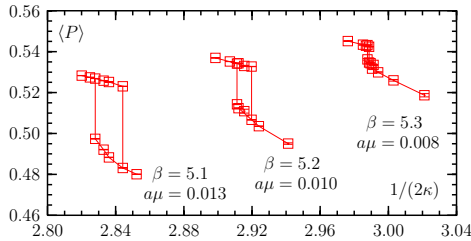

Figure 5: The plaquette expectation value $\langle P \rangle$ as a function of $1/(2\kappa)$ at three values of the lattice spacing (corresponding to the three values of β in the graph) we have simulated. We also indicate the values of $a\mu$ which are scaled with β such that $r_0\mu$ is roughly constant. The lines just connect the data points and only serve to guide the eye.

In the benchmark paper [58] we only used a single value of the lattice spacing, a single volume and only varied the quark mass. Also, we only looked at simple meson observables such as the pion mass and the pion decay constant which we compared to chiral perturbation theory predictions, see fig. 6 for the example of the pseudo scalar decay constant.

The fact that 300MeV pion masses could be reached and that by tuning only one parameter to reach maximal twist and hence automatic $O(a)$-improved of physical quantities, triggered a number of groups in Europe to join our effort of performing calculations with maximally twisted mass fermions. This eventually ended in the formation of the European Twisted Mass Collaboration (ETMC) which led to a very successful collaboration in the following years. It established a very broad research programme by addressing many interesting physical observables. One very important spin-off of this activity has been the calculation of quantities that are important for exploring hadron structure as focused
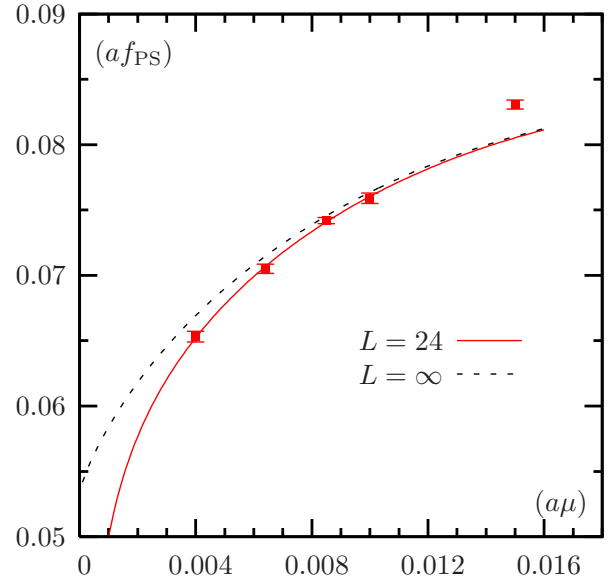

Figure 6: The graph shows af_{PS} as a function of bare twisted quark mass μ_q together with fits to χPT formula, see [58]. The figure shows a fit applied to the raw data on the $L = 24$ lattice at the 4 lowest values of μ_q. The finite size corrected result is represented by the dashed curve.

on in the work of ref. [5]. Another important spin-off has been the calculations at a non-zero temperature [81] which has been performed in this project. Both activities, the analysis of hadron structure and the twisted mass lattice QCD at non-zero temperature have significantly profited from simulations carried out in this work.

3.2. Algorithm and software development

It is important to emphasize that the success of this project relied to a large extend on the development of new algorithms and an efficient implementation of these algorithms on various computer platforms.

A major breakthrough has been the development of a Hybrid Monte Carlo algorithm [82] with mass preconditioning [83, 84] and multiple time step integrators with a corresponding distribution of different parts of the action on different time steps [62].

In fig. 7 we show the improvement that we could achieve. The solid line represents the cost scaling of previous implementations of the HMC algorithm as a function of the ratio of the pion to the ρ-meson mass. The curve is based on the formula given in ref. [85]

$$C = K \left(\frac{m_{PS}}{m_V} \right)^{-z_\pi} L^{z_L} \, a^{-z_a} \, , \tag{9}$$

where the constant K can be found in ref. [85] and $z_\pi = 6$, $z_L = 5$ and $z_a = 7$. The result of this com-
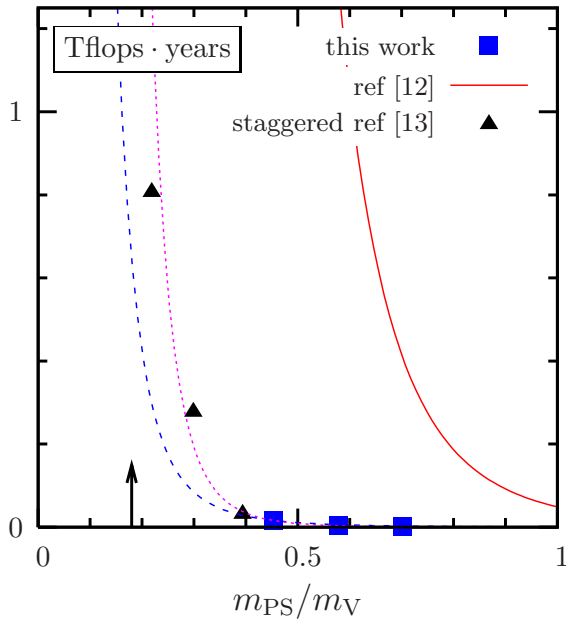
Figure 7: Computer resources needed to generate 1000 independent configurations of size $24^3 \times 40$ at a lattice spacing of about 0.08 fm in units of Tflops · years as a function of m_{PS}/m_V. We compare to the formula for the computational cost of eq. (9) [85] (solid line) by extrapolating our data with $(m_{PS}/m_V)^{-4}$ (dashed) and with $(m_{PS}/m_V)^{-6}$ (dotted), respectively. The arrow indicates the physical pion to rho meson mass ratio. Additionally, we add points from staggered simulations as were used for the corresponding plot in ref. [86]. Note that all the cost data were scaled to match a lattice time extend of $T = 40$.

parison is plotted in figure 7. The data points show the improvement of our new algorithm. The software of our algorithm, called tmLQCD, is documented in [87] and can be freely downloaded [88].

It is worth mentioning that at the same time we found our algorithmic improvement, also other groups found similar reductions of the algorithmic cost through alternative ideas [89, 90, 91]. This led to a general change in lattice QCD simulations and enabled simulations on large lattice sizes and small quark masses that were unthinkable before. Most advanced algorithmic improvements nowadays even lead to an almost flat scaling behaviour of the computational cost as a function of the pion mass, see [92].

Besides improving the algorithm itself, it is also necessary to implement the algorithm in an efficient way on super computers. In [93, 94] a description of the implementation of the tmLQCD software package is given, employing multi-threading and openMP, usage of instrinsics and tuning to an optimal mapping of the 4-dimensional lattice to the node network of the computer. In fig. 8 we show one example of the gain that can be achieved of carefully exploring and using the utilities

available on a supercomputer.

As mentioned before, tmLQCD includes optimisations for several modern supercomputer architectures, IBMs Blue Gene/Q, Intels SSE instruction set and the Aurora architecture. We also have an inverter and parts of the HMC implemented for NVIDIA GPUs.
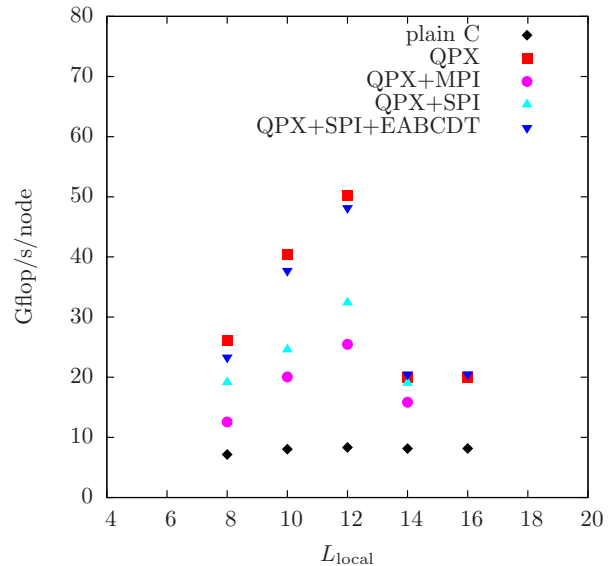

Figure 8: Single BG/Q node double precision performance of the hopping matrix in Gflop/s as a function of L_{local}. "Plain C" and "QPX" correspond to measurements with communication switched off using a plain C implementation and one including QPX instructions, respectively. The other points include communication, see also refs. [93, 94].

4. Simulations with $N_f = 2$ flavours of mass-degenerate quarks

Equipped with the improved HMC algorithm and an efficient implementation of the tmLQCD software suite, the ETMC performed simulations for $N_f = 2$ flavours of mass-degenerate light quarks for different values of the lattice spacing, lattice volumes and quark masses [58, 95, 48]. In this way, systematic effects from disretization and finite volume errors could be determined allowing thus for controlled results with a determination of systematic errors in a quantitative way.

As a first step, an analysis for the pion mass and the pion decay constant as a function of the quark mass has been performed by confronting these data to analytical expressions of chiral perturbation theory.

The formulae describing the chiral and continuum behaviour of f_{PS}, m_{PS} in infinite volume and leading $O(a^2)$

lattice spacing effects read [96, 97, 98]:

$$(r_0^\chi m_{\rm PS})^2 = (r_0^\chi)^2 \chi_\mu \left[1 + \xi \log\left(\frac{\chi_\mu}{\Lambda_3^2}\right) \right.$$
$$\left. + D_{m_{\rm PS}}(a/r_0^\chi)^2 + T_m^{\rm NNLO} \right], \qquad (10)$$

$$r_0^\chi f_{\rm PS} = r_0^\chi f_0 \left[1 - 2\xi \log\left(\frac{\chi_\mu}{\Lambda_4^2}\right) \right.$$
$$\left. + D_{f_{\rm PS}}(a/r_0^\chi)^2 + T_f^{\rm NNLO} \right], \qquad (11)$$

where $T_{m,f}^{\rm NNLO}$ denote the continuum NNLO χPT terms

$$T_m^{\rm NNLO} = \frac{17}{2}\xi^2 \left[\log\frac{\chi_\mu}{\Lambda_M^2} \right]^2 + 4\xi^2 k_M , \qquad (12)$$

$$T_f^{\rm NNLO} = -5\xi^2 \left[\log\frac{\chi_\mu}{\Lambda_F^2} \right]^2 + 4\xi^2 k_F , \qquad (13)$$

with

$$\log\frac{\Lambda_M^2}{\chi_\mu} = \frac{1}{51}\left(28\log\frac{\Lambda_1^2}{\chi_\mu} + 32\log\frac{\Lambda_2^2}{\chi_\mu} \right.$$
$$\left. - 9\log\frac{\Lambda_3^2}{\chi_\mu} + 49 \right), \qquad (14)$$

$$\log\frac{\Lambda_F^2}{\chi_\mu} = \frac{1}{30}\left(14\log\frac{\Lambda_1^2}{\chi_\mu} + 16\log\frac{\Lambda_2^2}{\chi_\mu} \right.$$
$$\left. + 6\log\frac{\Lambda_3^2}{\chi_\mu} - 6\log\frac{\Lambda_4^2}{\chi_\mu} + 23 \right), \qquad (15)$$

and we have defined

$$\xi \equiv \chi_\mu/(4\pi f_0)^2, \quad \chi_\mu \equiv 2B_0\mu_R, \qquad (16)$$

and

$$\mu_R \equiv \mu_q/Z_{\rm P}^{\overline{\rm MS}}(\mu = 2\,{\rm GeV}) . \qquad (17)$$

We use a normalisation such that $f_0 = \sqrt{2}F_0$, i.e. $f_\pi = 130.7$ MeV. For the finite size corrections we have used the formulae of refs. [99, 100].

An example for a chiral fit using the above formulae is shown in fig. 9. By performing a large variation of such fits, excluding certain data sets, using different orders of chiral perturbation theory or different kind of finite size corrections, the distribution for the fit parameters has been built. From the median of this distribution we determine the value of the fit parameter and from the width the systematic error. Our results can be found in table 2. As can be seen, the chiral fits allowed to determine a set of low energy constants with good statistical precision and a quantitative determination of systematic errors.

	median	statistical	systematic
$m_{u,d}$ [MeV]	3.54	(19)	$(+16-17)$
$\bar{\ell}_3$	3.50	(9)	$(+9-30)$
$\bar{\ell}_4$	4.66	(4)	$(+4-33)$
f_0 [MeV]	121.5	(0.1)	$(+1.1-0.1)$
B_0 [MeV]	2638	(149)	(± 132)
$|\Sigma|^{1/3}$ [MeV]	270	(5)	$(+3-4)$
f_π/f_0	1.0755	(6)	$(+8-94)$
$Z_{\rm P}(\beta = 3.90)$	0.434	(8)	$(+4-2)$
$Z_{\rm P}(\beta = 4.05)$	0.452	(9)	$(+3-9)$

Table 2: Summary of fit results. The first error is of statistical origin while the second, the asymmetric one, accounts for the systematic uncertainties. B_0, Σ and $m_{u,d}$ are renormalised in the $\overline{\rm MS}$ scheme at the renormalisation scale $\mu = 2$ GeV, as the values of $Z_{\rm P}$ are in the $\overline{\rm MS}$ scheme at scale 2 GeV. The scale is set by $f_\pi = 130.7$ MeV as done in ref. [58]. For a comparison to other recent lattice results we refer the reader to ref. [101].

5. Highlight results for $N_f = 2$ flavours

The set of gluon field configurations generated by ETMC for $N_f = 2$ flavours of mass-degenerate quarks at various values the lattice spacing, volume and quark masses served as a basis for the computation of many other physical quantities. In this section we will highlight those calculations that have been in the focus of the twisted mass research project within this transregional collaborative research center. In particular, we will discuss in this section the leading order hadronic contributions to the lepton anomalous magnetic moments, the pion scattering length and the ρ-meson resonance. Results concerning the investigation of the structure of hadrons and baryon masses will be addressed in a separate contribution [5].

5.1. Muon anomalous magnetic moment

The anomalous magnetic moment of the muon, a_μ, is considered to be an important benchmark quantity to test the standard model of particle interactions. Alternatively a_μ can be seen as a prime candidate observable to detect new physics beyond the standard model. The anomalous magnetic moment of the muon can be measured experimentally very precisely [102, 103]. It can also be computed precisely in the standard model, see e.g. the review [104]. Comparing experimental results and standard model calculations for a_μ reveals a discrepancy of about three σ which is persistent over many years now. The open question is, whether this discrepancy originates from some undetected effect in the experimental or theoretical determination of a_μ, or,
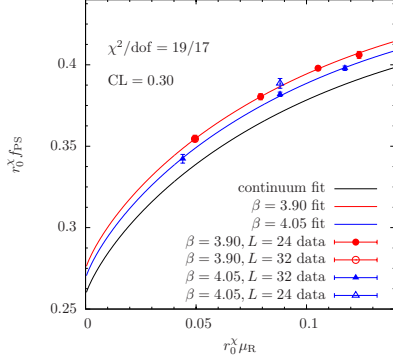
Figure 9: We show one example of a chiral fit for $r_0^\chi f_{PS}$ as a function of $r_0^\chi \mu_R$. Circles (triangles) represent data points from a lattice spacing of about $a = 0.09$fm ($a = 0.075$fm). The value of χ^2/dof obtained for this fit is 19/17. Note that in these figures we did not propagate the errors of r_0^χ and Z_P. When these errors are included the statistical significance of a^2-dependence of the data in the figures decreases.

somewhat more excitingly, whether it points to physics beyond the standard model.

The leading order hadronic vacuum polarisation contribution, a_μ^{hvp}, is a key ingredient in the calculation of a_μ. Presently, it also constitutes the largest source of uncertainty of the theoretical computation of a_μ. Since a_μ^{hvp} is of intrinsically non-perturbative nature, evidently a lattice QCD computation for this quantity is highly desirable.

The anomalous magnetic moment a_l of a lepton l can be written as a perturbative expansion in the electromagnetic coupling α. The leading order in α appears at order α^2 and can be written as [105]

$$a_l^{\text{hvp}} = \alpha^2 \int_0^\infty dQ^2 \frac{1}{Q^2} w(Q^2/m_l^2) \Pi_R(Q^2) . \qquad (18)$$

Here m_l denotes the mass of the lepton, Q is the Euclidean momentum and $w(Q^2/m_l^2)$ is a weight function, which is known. The combination $\Pi_R(Q^2) = \Pi(Q^2) - \Pi(0)$ is the renormalized hadronic vacuum polarization function $\Pi(Q^2)$. Finally, the vacuum polarization function is given by

$$\Pi_{\mu\nu}(Q) = \int d^4X\, e^{iQ \cdot X} \langle \Omega | T J_\mu(X) J_\nu(0) | \Omega \rangle \qquad (19)$$

and $J_\mu = \sum_f Q_f \bar{q}_f \gamma_\mu q_f$ is the hadronic contribution to the electromagnetic current.

In practise, the above given definition of the vacuum polarization function is used at various values of the squared momenta Q^2. The data in momentum space

are then parametrized by an ansatz using vector meson dominance and a polynomial,

$$\Pi_{\text{low}}(Q^2) = \sum_{i=1}^{M} \frac{f_i^2}{m_i^2 + Q^2} + \sum_{j=0}^{N-1} a_j (Q^2)^j , \qquad (20)$$

see ref. [106, 107]. For the case of an active strange and charm quark, as discussed below, we also employ Padé approximations [108]. The value of a_μ^{hvp} is then obtained at a fixed pion mass by integrating the function of eq. (20). Varying the number of terms in the fit ansatz, provides a measure of the size of the systematic errors in this procedure.

Following this strategy, the low lying set of data in fig. 10 are obtained. As can be seen, they are significantly and consistently below the experimental value. For these data, a phenomenological model has been developed [106] which allowed an extrapolation to the physical pion mass. However, this extrapolation has been afflicted with a substantial error for a_μ^{hvp}, about ten times bigger than the standard model error from a dispersive analysis.
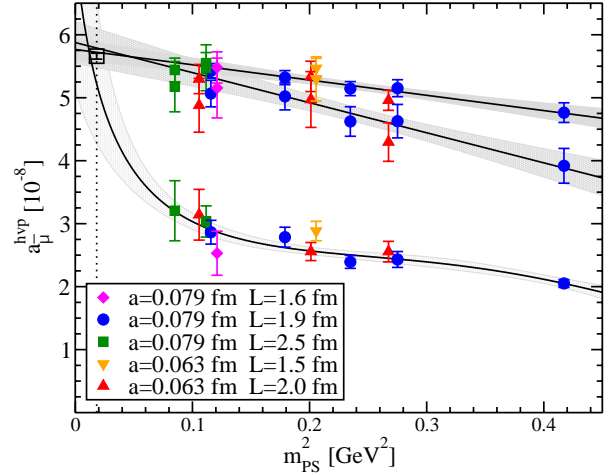

Figure 10: Comparison of the different methods described in the text to evaluate a_μ^{hvp}. The upper set of points are the results for $a_{\bar\mu}^{\text{hvp}}$ using $H = m_V$, the middle set use $H = f_V$, and the lower set correspond to the standard method, formally $H = 1$. The two lines are linear extrapolations of $a_{\bar\mu}^{\text{hvp}}$ and the curve is the phenomenological extrapolation of a_μ^{hvp}. The three methods agree at the physical point, denoted by the dashed line, and agree with the estimated two-flavor contribution to the experimental value.

The situation changed when it was realized in ref. [106] that a different definition of a_l^{hvp} can be used at unphysical values of the pion mass. The only condition for such an alternative definition must be that the standard definition is recovered at the physical value of

the pion mass. The definition that has been suggested in [106] reads

$$a_l^{\text{hvp}} = \alpha^2 \int_0^\infty dQ^2 \frac{1}{Q^2} w\left(\frac{Q^2 H_{\text{phys}}^2}{m_l^2 H^2}\right) \Pi_R(Q^2) \qquad (21)$$

where H is a hadronic quantity, evaluated at the (unphysical) pion mass used in the simulation. H_{phys} corresponds then to its physical value. The natural choice for our calculation is the vector meson mass, i.e. $H = m_V$. By construction we have then that $H(m_{PS} \to m_\pi) = H_{\text{phys}}$. The standard method can be reproduced by the choice $H = 1$, but choosing a dimensionful scale has the additional advantage that the explicit dependence on the lattice spacing is eliminated. At the same time, the renormalization condition that defines the physical limit is now given by the dimensionless ratio m_l/H_{phys} rather than m_l alone.

One reason why this modified method to compute a_l^{hvp} is supposed to work is the relation $a_{l,V} \approx g_V^2 m_l^2 / m_\rho^2$. Clearly, choosing $H = m_V$ takes out the pion mass dependence of the vector meson mass [109] and should lead to a much milder pion mass dependence of a_l^{hvp}. This is indeed seen in fig. 10. The data are moving much closer to the phenomenological value even at large pion masses. In addition, the pion mass dependence is very flat and perfectly consistent with a linear behaviour in the pion mass which allows for a controlled extrapolation to the physical pion mass and a correspondingly much smaller error.

This procedure has been carried through for the leading order contribution of all lepton anomalous magnetic moments and the following results are found,

$$\begin{aligned} a_{e,N_f=2}^{\text{hvp}} &= 1.513\,(43) \cdot 10^{-12}, \\ a_{\mu,N_f=2}^{\text{hvp}} &= 5.72\,(16) \cdot 10^{-8}, \\ a_{\tau,N_f=2}^{\text{hvp}} &= 2.650\,(54) \cdot 10^{-6}. \end{aligned} \qquad (22)$$

The significantly reduced errors for the a_l^{hvp} in eqns. (22) constitute a breakthrough in lattice QCD for a_l^{hvp} and the work of ref. [106] has been provided with the first Ken Wilson lattice award. In ref. [110] it was demonstrated that the strategy developed in [106] can be used for many other hadronic contributions of electroweak observables and much work is in progress to obtain results for these quantities.

5.2. $I = 2$ *pion scattering length and ρ-meson resonance*

As another usage of the generated configurations we calculated the s-wave pion-pion scattering length in the

isospin $I = 2$ channel in lattice QCD for pion masses ranging from 270 MeV to 480 MeV. This calculation is based on the finite volume method of refs. [111, 112, 113]. It relates the energy of a $(\pi\pi)$ state to the $I = 2$ elastic scattering length in infinite volume,

$$\begin{aligned} E_{\pi\pi}^{I=2} - 2m_\pi &= -\frac{4\pi a_{\pi\pi}^{I=2}}{m_\pi L^3}\left[1 + c_1 \frac{a_{\pi\pi}^{I=2}}{L} + c_2\left(\frac{a_{\pi\pi}^{I=2}}{L}\right)^2\right] \\ &+ O(L^{-6}) \end{aligned} \qquad (23)$$

where $c_1 = -2.837297$ and $c_2 = 6.375183$ are numerical constants.

The energy of the two pion state can be extracted from the exponential decay of a suitable $\pi\pi$ correlation function, see ref. [114]. Of course, the so obtained energies are obtained at unphysical values of the pion mass and need to be extrapolated to the physical pion mass. To this end, we have employed next to leading order continuum chiral perturbation theory [115],

$$\begin{aligned} m_\pi a_{\pi\pi}^{I=2} &= -\frac{m_\pi^2}{8\pi f_{\pi,\text{chi}}^2}\Bigg\{1 + \frac{m_\pi^2}{16\pi^2 f_{\pi,\text{chi}}^2}\Bigg[3\ln\left(\frac{m_\pi^2}{\mu^2}\right) \\ &\quad - 1 - l_{\pi\pi}^{I=2}(\mu)\Bigg]\Bigg\} \end{aligned} \qquad (24)$$

where $l_{\pi\pi}^{I=2}(\mu)$ is related to the Gasser-Leutwyler coefficients $\bar{l}(\mu)$ as

$$l_{\pi\pi}^{I=2} = \frac{4}{3}\bar{l}_1 + \frac{8}{3}\bar{l}_2 - \frac{1}{2}\bar{l}_3 - 2\bar{l}_4. \qquad (25)$$

Using these formulae, we have performed a chiral extrapolation of our results and in fig. 11 we show the good quality of this chiral extrapolation.

Most of our results have been obtained at a lattice spacing of 0.086 fm. Additionally, we have checked for lattice artifacts with one calculation at a finer lattice spacing of 0.067 fm with the result that lattice spacing effects are small. At the physical pion mass, we find for the scattering length $m_\pi a_{\pi\pi}^{I=2} = -0.04367\,(28)(36)$ and for the corresponding low energy constant $l_{\pi\pi}^{I=2} = 4.65\,(.85)(1.07)$ at a scale of $\mu = f_{\pi,\text{phys}}$. The first error is statistical and the second is our estimate of systematic effects.

The successful calculation of the $I = 2$ scattering amplitude motivated to perform a pilot study [109] to also extract the ρ resonance parameters in lattice QCD. To this end, we performed a non-perturbative lattice calculation of the P-wave pion-pion scattering phase in the ρ-meson decay channel using two flavors of maximally twisted mass fermions at pion masses ranging from 480
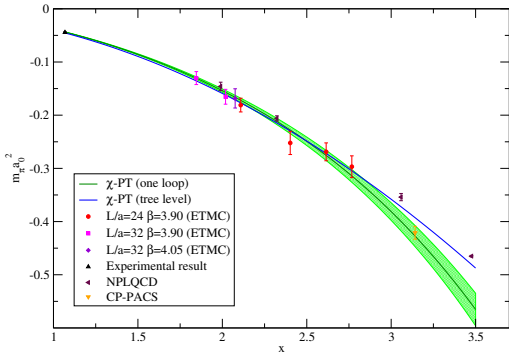
Figure 11: Chiral extrapolation for the I=2 pion-pion scattering length. The results in this work are shown together with the lattice calculations of NPLQCD [116, 117] and CP-PACS [118] and the experimental analysis from refs. [119].
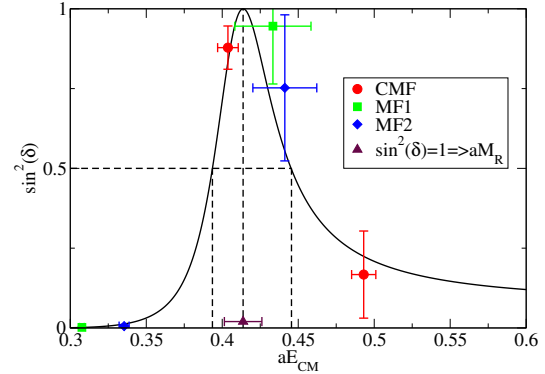

Figure 12: We show one example of the scattering phases calculated in the center of mass frame (CMF) and two moving frames (MF1 and MF2) together with the fits to the effective range formula eq. (26). At the position where the scattering phase passes $\pi/2$, the resonance mass m_ρ (denoted as aM_R in the graph) is determined. Through the fit, the coupling constant $g_{\rho\pi\pi}$ and decay width Γ_ρ are also extracted.

MeV to 290 MeV. Making use of the finite size method developed in ref. [111, 112, 113], we have evaluated the pion-pion scattering phase in the center-of-mass frame and two moving frames.

In order to describe the energy dependence of the scattering phase we use the effective range formula

$$\tan \delta_1 = \frac{g_{\rho\pi\pi}^2}{6\pi} \frac{p^3}{E_{CM}(m_\rho^2 - E_{CM}^2)} \qquad (26)$$

$$p = \sqrt{E_{CM}^2/4 - m_\pi^2} \qquad (27)$$

with E_{CM} the center of mass energy. The scattering phase and a fit to eq. (26) is shown in fig. 12. As can be seen, the energy range we are using covers the resonance region and the effective range formula of eq. (26) describes the data rather well. From the fit, we can then read off the ρ-meson resonance mass and its decay width. After performing a chiral extrapolation using the z-expansion [120, 121], we find a ρ-meson mass $m_{\rho,\text{phys}} = 0.850(35)$ GeV and $\Gamma_{\rho,\text{phys}} = 0.166(49)$ GeV. Clearly the accuracy of these numbers cannot yet match the experimental one. However, it needs to be stressed that this work to determine resonance parameters was one of the first of its kind and demonstrated that resonance parameters can be extracted from lattice calculations. The idea of using several moving frames as pioneered in our work has then been utilized in more recent publications and much more precise results at the one percent level could be obtained, see e.g. ref. [122] and the review in ref. [123]

6. Renormalization

Many observables that are computed in lattice QCD need a renormalization which should be performed ideally non-perturbatively. We therefore carried through a dedicated programme for computing renormalization constants of bilinear quark operators and also operators appearing in matrix elements and form factors needed for exploring hadron structure [124, 125, 126, 127].

In particular, we calculated the scale-independent renormalization constants Z_V, Z_A and the ratio Z_P/Z_S employing the RI-MOM approach [128] as well as many other renormalization constants that were needed. In the evaluation of these renormalization constants leading discretization effects of $O(g^2a^2)$, computed in one-loop perturbation theory, are explicitly subtracted from the RI-MOM estimates.

In fig. 13 we show the example of the renormalization constant of the vector current, Z_V as a function of the lattice momentum. Ideally, Z_V should show a constant behaviour as function of a^2p^2. However, as can be seen from the graph, the raw data (empty circles in the graph) deviate from being constant.

When the leading order cut-off effects in lattice perturbation theory $O(g^2a^2)$ are subtracted, represented by the filled symbols in fig. 13, we find that Z_V is constant as a function of a^2p^2 allowing thus to read off the renormalization constant. It needs to be mentioned that the leading order lattice perturbation theory corrections not always give such an improvement, but nevertheless

computing the renormalization constants with and without perturbative subtractions provides a valuable cross-check of the final results.
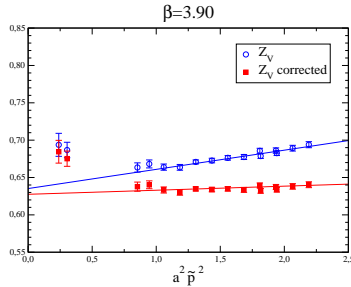

Figure 13: The renormalization constant $Z_V(1/a; a^2 p^2)$ at a lattice spacing of $a \approx 0.09$fm, evaluated at the reference scale $\mu_0 = 1/a$, plotted against the initial renormalization scale $a^2 p^2$. Filled squares (empty circles) are results obtained with (without) the subtraction of the $O(g^2 a^2)$ discretization effects computed in perturbation theory, see [129]. The solid lines are linear fits to the data.

The lattice results of the renormalization constants obtained in the RI-MOM scheme need to be converted to the $\overline{\text{MS}}$ scheme. In the case of scale μ dependent renormalization constants, they also need to be be run to a certain reference scale, with typically $\mu = 2$GeV. For both, the conversion and the evolution we have used the highest available loop order that has been computed [130, 131, 132].

Besides the RI-MOM scheme, which has been our working horse to compute renormalization constants, we also explored [133, 134] the Schrödinger functional scheme [135, 136, 137] which has been generalized to twisted mass fermions in ref. [138]. In addition, we performed a calculation in the coordinate (X-space) renormalization scheme [139, 140]. Both of these approaches have the advantage to lead to renormalization constants in a gauge invariant way.

For the X-space method, we looked [140] at various current-current correlation functions and tried to find a window at small distances where safe contact to perturbation theory could be made. This then in turn allowed the computation of the corresponding renormalization constants and we found a full agreement with results from the RI-MOM scheme, having thus a completely independent cross-check at hand.

For the Schrödinger functional scheme we could demonstrate that this setup, in principle, can be used for maximally twisted mass fermions without destroying the property of automatic $O(a)$-improvement [133, 134]. However, the Schödinger functional scheme was then in the following not used in practice since this ap-

proach would have required a new set of simulations with the corresponding rather involved analysis.

7. Activating the strange and the charm quark

The results so far discussed have been obtained with $N_f = 2$ flavours of mass-degenerate quarks. Encouraged by the results of these $N_f = 2$ simulations, we decided to move on to also include the strange and the charm quark as active degrees of freedom in our computations [141, 142, 143], see ref. [144] for a review of this situation. The action for this $N_f = 2 + 1 + 1$ setup is given by [12, 145]

$$
\begin{aligned}
S_h \;=\; & a^4 \sum_x \Big\{ \bar{\chi}_h(x) \Big[D[U] + m_{q,h} \\
& + i\mu_\sigma \gamma_5 \tau_1 + \mu_\delta \tau_3 \Big] \chi_h(x) \Big\} \,,
\end{aligned}
\tag{28}
$$

where $m_{q,h}$ is the untwisted bare quark mass for the heavy doublet, μ_σ the bare twisted mass – the twist is this time along the τ_1 direction – and μ_δ the mass splitting along the τ_3 direction.

One very important observation is that with the action in eq. (28) automatic $O(a)$-improvement can be realized by setting the bare Wilson quark mass $m_{q,h}$ to the same value as the tuned bare Wilson quark mass in the light sector. Clearly, this significantly eases the tuning of the theory to obtain the desired $O(a^2)$ continuum limit scaling behaviour.

The bare mass parameters μ_σ and μ_δ of the non-degenerate heavy doublet are related to the physical renormalised strange and charm quark masses via [146]

$$
\begin{aligned}
(m_s)_{\text{R}} \;&=\; Z_{\text{P}}^{-1} \left(\mu_\sigma - Z_{\text{P}}/Z_{\text{S}} \, \mu_\delta \right), \\
(m_c)_{\text{R}} \;&=\; Z_{\text{P}}^{-1} \left(\mu_\sigma + Z_{\text{P}}/Z_{\text{S}} \, \mu_\delta \right),
\end{aligned}
\tag{29}
$$

where Z_{P} and Z_{S} are the renormalisation constants of the pseudo scalar and scalar quark densities, respectively, computed in the mass-less standard Wilson theory.

It needs to be stressed that the determinant associated with eq. (28) is still positive for all values of μ_σ and μ_δ that are used in practical simulations. Thus, the addition of the strange and charm quarks works well within the twisted mass setup and, in fact, adding a doublet of quarks is very natural for twisted mass fermions.

In ref. [141] we have carried through the very first simulations with active strange and charm quarks. There we could demonstrate that computations in this setup are feasible and that tuning the theory to maximal twist can be achieved. In addition, a strategy has been outlined to calculate a variety of meson masses and decay constants. The technology of ref. [141] has been

further developed in [142, 143] and a comprehensive analysis of the the light meson and the heavy light meson sectors have been performed. See also ref. [144] for a review of simulations with active up, down, strange and charm quarks.

As a first step, we performed very similar chiral fits to the obtained pseudo scalar decay constants and masses. Having data at various lattice spacings and volumes, quantitative estimates of the size of these systematic effects could be given. In table 3 we give a comparison of the extracted low energy constants for both, the $N_f = 2$ and the $N_f = 2 + 1 + 1$ setups. The compatibility of the values of the low energy constants given in the table reveals that for the light meson sector the effects of an active strange and charm quark are not visible within the precision we could reach.

	$N_f = 2$	$N_f = 2 + 1 + 1$
$\bar{\ell}_3$	3.70(27)	3.50(31)
$\bar{\ell}_4$	4.67(10)	4.66(33)
f_π/f_0	1.076(3)	1.076(9)
Σ[MeV]	299(40)	325(10)
$\langle r^2 \rangle_s^{\text{NLO}}$ [fm^2]	0.710(28)	0.715(77)

Table 3: A comparison of the values of low energy constants of the chiral effective Lagrangian from $N_f = 2$ and $N_f = 2 + 1 + 1$ flavour simulations of maximally twisted mass simulations.

The major drawback of the twisted mass setup in the heavy quark sector is that there parity and flavour are not good quantum numbers making it thus difficult to extract, e.g., the Kaon and, in particular, the D-meson masses. We have investigated three methods to determine m_K and m_D in $N_f = 2 + 1 + 1$ twisted mass lattice QCD and have explored strategies to extract the desired states. To this end we have developed three distinct methods all of which exploit the exponential fall-off of correlation matrices for suitably chosen heavy-light meson creation operators. Method 1 amounts to solving a generalized eigenvalue problem, method 2 is equivalent to fitting a linear superposition of exponentials and method 3 transforms the correlators to the physical basis by means of the twist rotation. In table 4 we give a comparison of the so extracted Kaon mass (m_K) and the D-meson mass (m_D) for one gluon field ensemble.

Although in the work of ref. [143] we could demonstrate that it is feasible to address the parity and isospin breaking effects for twisted mass fermions in the heavy quark sector, the calculations are nevertheless rather difficult and cumbersome. We have therefore often used a different action in the valence sector, so-called

	Method 1	Method 2	Method 3
am_K	0.2567(2)	0.25554(88)	0.25668(35)
am_D	0.922(11)	0.901(21)	0.909(22)

Table 4: Comparison of the results for m_K and m_D obtained with the three methods mentioned in the text and discussed in ref. [143].

Osterwalder-Seiler fermions [147]. The corresponding Dirac operator is given by

$$
\begin{aligned}
D_{\text{OS},\pm} &= m_q \pm i\mu\gamma_5 \\
&+ \frac{1}{2}\gamma_\mu\left[\nabla_\mu + \nabla_\mu^*\right] - a\frac{1}{2}\nabla_\mu^*\nabla_\mu
\end{aligned}
\tag{30}
$$

and amounts to take only one (upper or lower flavour) component of the twisted mass Dirac operator. In this way the isospin violating effects are completely avoided which substantially helps in the simulations. In addition, the bare quark mass m_q in eq. (30) is again set to the tuned quark mass in the light quark sector to keep automatic $O(a)$-improvement. Clearly, in this way a mixed action is used for analyzing the heavy quark sector. However, the twisted mass operator and the OS operator are so closely related that only very small unitarity violations are to be expected which has been confirmed in the calculations where OS fermions have been employed.

Unfortunately, OS fermions cannot be used straightforwardly in a simulation since the corresponding determinant is not necessarily positive, restricting its use therefore as a tool to extract physics in the heavy quark sector.

8. Selected results from twisted mass fermion simulations

The set of maximally twisted mass fermions both, for $N_f = 2$ and $N_f = 2 + 1 + 1$ flavours of quarks led to a number of physical quantities that were computed on the corresponding gluon field configurations. In the following, we will describe a few of the computations.

8.1. Baryon spectrum

A benchmark calculation in lattice QCD is the octet and decuplet baryon mass spectrum. We performed such calculations first with only $N_f = 2$ mass-degenerate quark flavours [51, 148]. Here we found a nice agreement between the experimentally measured octet spectrum and our lattice calculations.

We also calculated the spectra with the first two quark generations active in the simulations [149]. We show in fig. 14 the outcome of this computation. As can be seen, our lattice QCD results indeed reproduce the baryon spectrum which nicely demonstrates that we control the simulations in our setup. In [149] we have extended these calculations also to the Charm spin-1/2 and the Charm spin-3/2 baryon masses, finding again agreement with the experimentally determined masses. However, it is worth stressing that also predictions are provided for the mass of the doubly charmed Ξ_{cc}^*, as well as of the doubly and triply charmed Ωs that have not yet been determined experimentally.
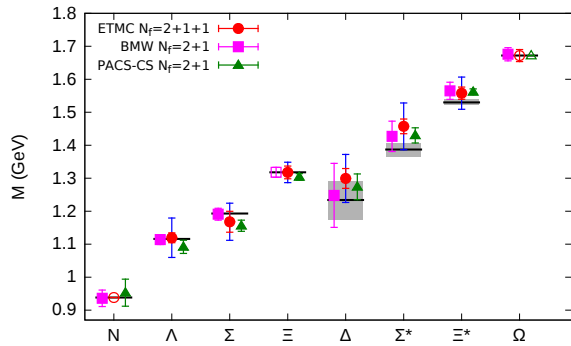
Figure 14: The octet and decuplet baryon masses obtained at the physical point and the experimental masses [150] shown by the horizontal bands. For most baryons the band is too small to be visible. For the twisted mass results of this work (red circles) the chiral extrapolation was performed using the leading order HBχPT. In our results, the statistical error is shown in red, whereas the blue error bar includes the statistical error and the systematic errors due to the chiral extrapolation and due to the tuning added in quadrature. Results using clover fermions from BMW [151] are shown in magenta squares and from PACS-CS [152] with green triangles. Open symbols are used wherever the mass was used as input to the calculations.

8.2. Chiral condensate

The chiral condensate Σ is the order parameter of spontaneous chiral symmetry breaking in QCD which is a fundamental and inherently non-perturbative phenomenon. Having an a-priori test directly from QCD, whether the chiral condensate is non-zero and determining its value quantitatively is therefore a prime target of lattice QCD calculations.

In this work, we have explored several strategies to determine the chiral condensate. The most natural way has been already explained in previous paragraphs and consists of performing fits to formulae from chiral perturbation theory to the pion decay constant and the pion mass. In these fits the chiral condensate appears as one

of the low energy constants of the effective chiral Lagrangian, see eq. (11). In fig. 6 and fig. 9 we show the quality of such fits and in table 3 we have provided the values of B_0 which is related to the chiral condensate through the formula

$$\Sigma = \frac{B_0 f_0^2}{2} \tag{31}$$

where f_0 is the pion decay constant in the chiral limit.

A completely alternative way is the exploitation of the Banks-Casher relation which reads

$$\frac{\Sigma}{\pi} = \lim_{\lambda \to 0} \lim_{m \to 0} \lim_{V \to \infty} \rho(\lambda, m) \tag{32}$$

where $\rho(\lambda, m)$ is the eigenvalue density,

$$\rho(\lambda, m) = \frac{1}{V} \sum_{k=1}^{\infty} \langle \delta(\lambda - \lambda_k) \rangle . \tag{33}$$

A conceptually clean way to make use of the Banks-Casher relation [153], which at the same time will lead to a practical procedure, is through the mode number,

$$
\begin{aligned}
\nu(M, m) &= V \int_{-\Lambda}^{\Lambda} d\lambda \rho(\lambda, m), \\
\Lambda &= \sqrt{M^2 - m^2}
\end{aligned}
\tag{34}
$$

which is the number of eigenvalues below a certain threshold parameter Λ. The parameter M is to some extent arbitrary and will be chosen such that a linear regime in the mode number as function of M can be established, since the chiral condensate can be obtained then from the slope of the mode number as function of M [154],

$$\Sigma \propto \partial/\partial M \nu(M, m) . \tag{35}$$

Another important result is that the mode number is a renormalization invariant, $\nu(m, M) = \nu_{\text{ren}}(m_{\text{ren}}, M_{\text{ren}})$ such that the renormalized chiral condensate can be obtained directly [154].

The essential quantity entering the computation of the chiral condensate is the spectral sum

$$\sigma_k(\mu, m_q) = \langle \text{Tr} \left(D_m^\dagger D_m + \mu^2 \right)^{-k} \rangle \tag{36}$$

which can be related to the mode number through

$$\sigma_k(\mu, m_q) = \int_0^\infty dM \nu(M, m_q) \frac{2kM}{(M^2 + \mu^2)^{k+1}} \tag{37}$$

which in turn can be expressed to density chains

$$\sigma_3(\mu, m_q) = a^{24} \sum_{x_1,\dots,x_6} \langle P_{12}^+(x_1) P_{23}^-(x_2) \dots P_{61}^-(x_6) \rangle \quad (38)$$

with the pseudo scalar currents

$$P_{ij}^\pm = \bar{\psi}_i \gamma_5 \tau^\pm \psi_j \,, \qquad (39)$$

where i, j denote different flavour doublets and $\tau^\pm$ acts on such a flavour doublet. The essential point for using the density chains of eq. (39) is that they lead to a conceptually very clean definition of the chiral condensate [154], and of the topological susceptibility [155, 156, 157] discussed later, which is free of divergencies. On the practical side, the mode number is computed by stochastically calculating the number of eigenvalues below the threshold parameter M, see ref. [154].

In this work, we have computed the chiral condensate [158] with the above sketched method using gluon field configurations for $N_f = 2$ and $N_f = 2 + 1 + 1$ flavours of quarks in the maximally twisted mass setup. For each ensemble of gluon field configurations we have performed a detailed study to identify the linear regime in M of the mode number. From the slope of this linear region we then have extracted the chiral condensate through

$$\Sigma_R = \frac{\pi}{2V} \sqrt{1 - \left(\frac{\mu_R}{M_R}\right)^2} \frac{\partial}{\partial M_R} \nu_R(M_R, \mu_R) \,. \qquad (40)$$

Having obtained in this way the renormalized chiral condensate at various quark masses, we perform fits for a fixed value of the lattice spacing using the NLO order of chiral perturbation theory,

$$\begin{aligned}
\frac{\Sigma(m, M)}{\Sigma} &= 1 - \frac{m\Sigma}{16\pi^2 F^4} \left\{ 3\ln \frac{\Lambda\Sigma}{\bar{\mu}^2 F^2} \right. \\
&+ \ln(1 + m^2/\Lambda^2) \\
&+ \left. \frac{m}{\Lambda} \text{atan} \frac{\Lambda}{m} + \frac{\Lambda}{m} \text{atan} \frac{m}{\Lambda} + \text{const} \right\} \quad (41)
\end{aligned}$$

to extrapolate to the chiral, mass-less limit.

In refs. [159, 160] it has been shown that the density chains, although afflicted by short distance contributions, are $O(a)$ improved such that we can perform a continuum limit extrapolation quadratically in the lattice spacing. The inlet in fig. 15 shows the continuum limit extrapolation. The analysis for the case of $N_f = 2 + 1 + 1$ flavours have been repeated by us also for only $N_f = 2$ flavours of quarks using the same strategy.
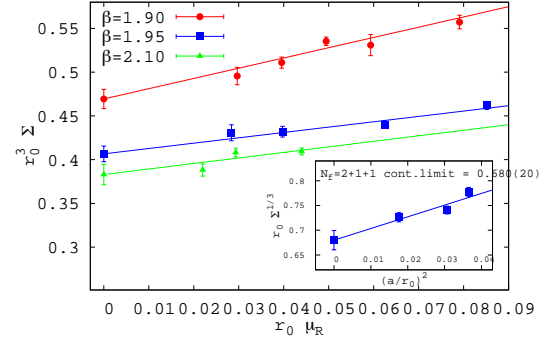

Figure 15: Chiral and continuum extrapolations of the chiral condensate for $N_f = 2 + 1 + 1$ flavours of active quarks.

In table 5 we give a comparison of the chiral condensate from various collaborations. To select the results, we have demanded that the results were obtained after a chiral and continuum extrapolation in order to achieve a comparable situation. Note that the values for the chiral condensate can differ significantly between different collaborations. This problem can be traced back to originate manly from the problem of setting the physical scale in lattice QCD calculations as discussed in [161].

group	$\Sigma^{1/3}$ MeV ($\overline{MS}$(2GeV))	error
1	299.9	7
2	298.1	8.7
3	263	(3)(4)
4	256	6
5	278	6
6	281.5	7.9
7	272.3	1.8
8	269.9	6.5
9	299	39
10	283	2

Table 5: Legend: 1.This work $N_f = 2$, 2.This work $N_f = 2 + 1 + 1$, 3. CLS [162], 4. RBC-UKQCD [163], 5. MILC [164], 6. MILC [165], 7. BMW [166], 8. ETMC [48], 9. ETMC [167], 10. HPQCD [168]

As mentioned above, there are still more methods to compute the chiral condensate. One can use the quark propagator itself on Landau gauge fixed configurations and confront the momentum dependence with continuum perturbation theory [169]. This allows for a test of the applicability of perturbation theory and a stable extraction of the chiral condensate which is moreover

fully compatible with the other results in table 5 where is appears as label 9.

Another possibility is the exploration of the so-called ϵ-regime of chiral perturbation theory [170, 171]. Here, one chooses the unphysical situation of the pion Compton wave length to be larger than the extent of the lattice. The corresponding strong finite size effects can then be described by an effective chiral Lagrangian which is parametrized by the low energy constants of chiral perturbation theory among which is the chiral condensate. This approach has been tested first in the quenched approximation [23] and has been employed for twisted mass fermions in [172].

Finally, one can also look at the eigenvalue distributions of the low lying eigenvalues of the lattice Dirac operator used [29]. These distributions are described by random matrix theory, see ref. [173] for the general case of Wilson fermions and ref. [174] for the special case of twisted mass fermions. The distributions of the low-lying eigenvalues have again the chiral condensate as a free parameter which can be obtained through a fit to the analytical predictions of random matrix theory. This approach has been tested in the quenched approximation for twisted mass fermions [26], see also [175] for the case of clover improved Wilson fermions. Work confronting random matrix theory predictions with numerical results using twisted mass fermions with active quarks is ongoing. It is worth mentioning that for the just started computations at the physical point making use of the low-lying eigenvalue spectrum is expected to be a good strategy to compute the chiral condensate.

8.3. Topology susceptibility

In a similar way as discussed above for the chiral condensate, also the topological susceptibility can be expressed by density chains [156, 157] through

$$\chi_{top} = \mu^6 \, \sigma_{2;1} \equiv \frac{\langle Q^2 \rangle}{V}, \qquad (42)$$

where:

$$\sigma_{2;1}(\mu) = a^{20} \sum_{x_1...x_5} \langle S^+_{41}(x_1) \, P^-_{12}(x_2) \, P^+_{23}(x_3)$$
$$P^-_{34}(x_4) \, S^+_{56}(x_5) \, P^-_{65}(0) \rangle . \qquad (43)$$

Here we introduced the currents and $S^{\pm}_{ij} = \bar{\chi}_i \tau^{\pm} \chi_j$ and $P^{\pm}_{ij} = \bar{\chi}_i \tau^{\pm} \gamma_5 \chi_j$, V is the volume and μ denotes the twisted quark mass.

Again, the essential advantage of this definition is that through eq. (42) a well defined, divergence free expression for the topological susceptibility can be obtained. As described in refs. [157] the density chains can be

evaluated stochastically by the method of spectral projectors. We applied this method for maximally twisted mass fermions [176, 159] and show in fig. 16 the obtained values of the topological susceptibility as a function of the renormalized quark mass at various values of the lattice spacing.

Fitting these data using a simple linear, leading order chiral perturbation theory ansatz, $\chi_{top} = \frac{\Sigma \mu_l}{N_f}$, we find a value for the chiral condensate, in units of the r_0, $r_0 \Sigma^{1/3} = 0.651(61)$. This result is in agreement with the above discussed direct determination from the mode number on the same set of gauge field ensembles, i.e. $r_0 \Sigma^{1/3} = 0.680(20)(21)$ [158], indicating that LOχPT describes the quark mass dependence of the topological susceptibility at least within the rather large errors of our results. In [159] we could demonstrate that also the topological susceptibility defined in eq.(42) is $O(a)$-improved such that lattice spacing artefacts only appear in $O(a^2)$.

It needs to be stressed, though, that the topological susceptibility is affected by substantial statistical fluctuations necessitating long Monte Carlo histories. With typical parameter values of Lattice QCD simulations nowadays, i.e. lattice spacings of $0.05\,\text{fm} \lesssim a \lesssim 0.1\,\text{fm}$ and lengths of Monte Carlo runs of $O(5000)$ trajectories with auto correlation times $\tau_{int} = O(10) - -O(500)$ trajectories, it is very difficult to obtain errors smaller than 10-15% for a given ensemble. It is important to note that this is not a property of the method used here, but of the gauge field configurations themselves and as such can not be easily overcome, i.e. without running very long simulations. Also, there is an additional problem with a substantially increasing auto correlation time when approaching the continuum limit [177] which manifests itself in the topological charge as a very sensitive quantity for detecting this very slow mode.
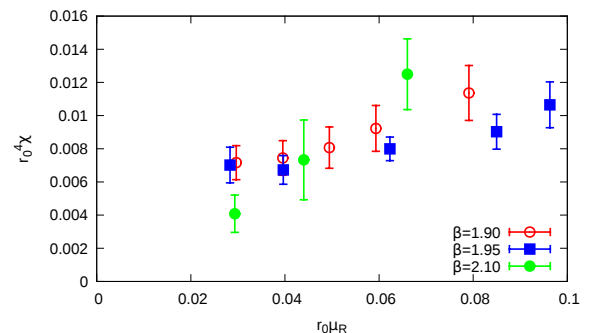

Figure 16: The quark mass dependence of the topological susceptibility.

8.4. Witten-Veneziano relation

The topological susceptibility is also a key ingredient in the Witten Veneziano formula. It relates the masses of the Kaon, η and η' mesons to the topological susceptibility at infinite (quenched) quark masses, χ_∞, and reads

$$\frac{f_\pi^2}{4N_f}\left(m_\eta^2 + m_{\eta'}^2 - 2m_K^2\right) = \chi_\infty, \tag{44}$$

where f_π is the pion decay constant.

The formula is obtained by taking the large colour, N_c limit. In particular, in Ref. [178], the 't Hooft limit ($N_c \to \infty$, while $g^2 N_c$ and N_f are kept fixed) is taken. Alternatively, an expansion in $u = N_f/N_c$ around $u = 0$ can be used as done in ref. [179]. The formula can also be obtained through the study of anomalous flavor-singlet Ward-Takahashi identities in the limit $u \to 0$ [180].

In ref. [181, 182, 183] the η and η' meson masses have been determined to a good accuracy. This is a highly non-trivial achievement since the correlator, from which the η' mass is extracted, receives contributions from disconnected graphs. Employing special techniques, in [181, 182] this difficulty could be partially avoided.

In order to obtain the quenched topological susceptibility, χ_∞, a dedicated computation has been performed. Employing the technique of the spectral projectors, results for χ_∞ could be obtained, such that a continuum limit could be carried out, see fig. 17. It is important to remark that all quenched simulations have been performed in such a way that the physical situation, which has been used to compute the meson masses, have been matched, see [142].
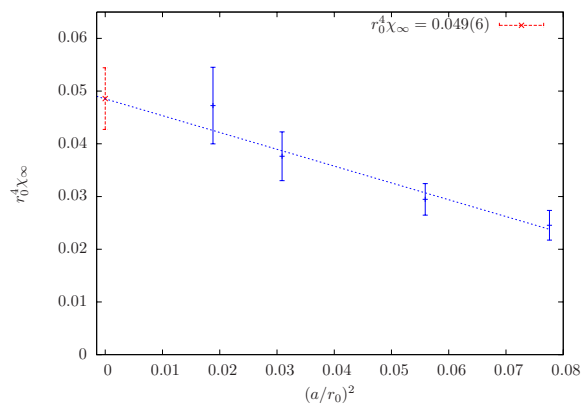

Figure 17: Continuum limit extrapolation of χ_∞ as a function of $(a/r_0)^2$ for the quenched ensembles used in this work.

In table 6 we give a comparison of the combination of masses needed for the Witten-Veneziano formula and

the quenched topological susceptibility. In units of r_0 we find a very nice agreement, showing that in lattice units the formula indeed holds. Since in [182] it has been demonstrated that at the physical value of the pion mass also the meson masses entering the Witten-Veneziano formula agree with their experimental counterparts, we conclude that the Witten Veneziano formula is indeed correct.

This is a most remarkable result since the validity of the Witten-Veneziano formula, as demonstrated by our non-perturbative lattice computations, provides a strong confirmation that the heavy mass of the η' meson is of topological nature.

$r_0 m_\eta$	$r_0 m_{\eta'}$	$r_0 m_K$	$r_0 f_\pi$
1.256(22)	2.29(0.21)	1.13476(5)	0.312(11)
$r_0^4 \frac{f_\pi^2}{4N_f}\left(m_\eta^2 + m_{\eta'}^2 - 2m_K^2\right) = 0.043(4)$			
$r_0^4 \chi_\infty = 0.049(6)$			

Table 6: Lattice results of the meson masses and the corresponding left-hand side of the Witten-Veneziano formula. χ_∞ is the topological susceptibility in the pure gauge theory computed using spectral projectors.

8.5. $g_\mu - 2$

Within this work, we have provided the first four-flavour lattice calculation [107] of the leading-order hadronic vacuum polarisation contribution to the anomalous magnetic moment of the muon, a_μ^{hvp}. Several light quark masses are used in order to yield a controlled extrapolation to the physical pion mass. In addition, three lattice spacings are used to examine lattice artefacts and several different volumes to check for finite-size effects. Including the complete first two generations of quarks is important for two reasons. The first is that the charm quark contribution to a_μ^{hvp} is of the same order as the light-by-light contribution. Hence, at the level when this light-by-light contribution becomes important to be included the charm quark contribution should be know to a sufficient accuracy. Second, a four flavour analysis of a_μ^{hvp} avoids any ambiguity in the disentanglement of different flavour contributions to a_μ^{hvp}. Therefore, a full four flavour computation of a_μ^{hvp} allows for a direct comparison with phenomenological determinations of this quantity.

Using the ensembles generated with $N_f = 2 + 1 + 1$ flavours of active quarks, the same strategy as explained in section 5.1 has been used to determine the leading order hadronic contributions to a_μ^{hvp}. The different flavour contributions are listed in table 7. We note that in another work [184] also the different flavour contributions

are listed. We find a full agreement with the numbers obtained in ref. [184].

$a_{\mu,\text{up,down}}^{\text{hvp}}$	$a_{\mu,\text{strange}}^{\text{hvp}}$	$a_{\mu,\text{charm}}^{\text{hvp}}$
$5.67(11) \cdot 10^{-8}$	$5.36(19) \cdot 10^{-9}$	$1.418(61) \cdot 10^{-9}$

Table 7: A comparison of the different flavour contributions for the leading order hadronic contribution to the muon anomalous magnetic moment. The strange and charm quark contributions are taken from ref. [4].

We also performed a comprehensive analysis of the systematic errors in the evaluation of a_μ^{hvp}. In table 8 we list the systematic errors originating from different fit intervals to extract the ρ-meson mass and employing different fit ansaetze, i.e., different numbers of terms in eq. (20). Investigating finite volume effect, the matching condition to find the physical Kaon and D-meson masses and using different active strange and charm quark masses lead to negligible systematic effects. A particular emphasis has been laid on dis-connected contributions. Here, a high statistics analysis has been carried out and the conclusion is that within the statistical error, the dis-connected contributions are negligible. This finding has been strengthened by a computation of the dis-connected contribution using the local vector current which provides an accurate determination of the dis-connected contribution [4].

Δ_V	$0.13 \cdot 10^{-8}$
Δ_{fit}	$0.12 \cdot 10^{-8}$

Table 8: Summary of systematic uncertainties. Δ_V is the systematic uncertainty from the choice of fit range for the vector mesons. Δ_{fit} is the uncertainty from using different fit ansätze for fitting the vacuum polarization function.

Taking the statistical and systematic errors into account, we find

$$a_\mu^{\text{hvp}} = 6.74(21)(18) \cdot 10^{-8} \tag{45}$$

where the first error is statistical and the second error is from systematic uncertainties. We compare the result of eq. (45) with the extraction from dispersion relations in fig. 18. As can be seen, the value of a_μ^{hvp} is fully compatible with the phenomenological extractions while the error is still larger. Nevertheless, it is clear that the error can be reduced in the future by employing a larger statistics and new methods like the all-mode-averaging approach of ref. [185, 186].
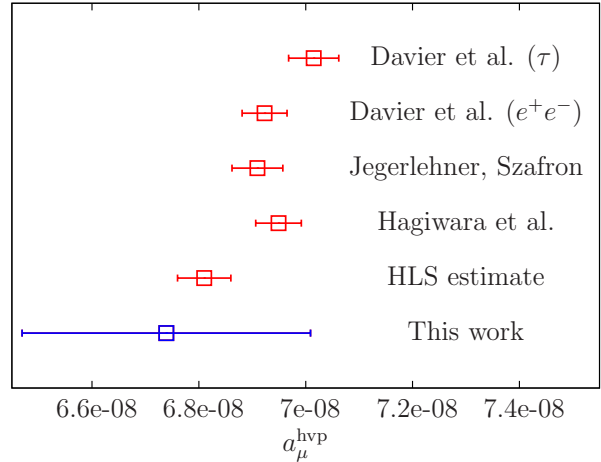

Figure 18: Comparison of our first four-flavour lattice result of a_μ^{hvp} with different results based on dispersion relations: Davier et al. [187], Jegerlehner and Szafron [188], Hagiwara et al. [189], and HLS [190]

8.6. Method of analytical continuation

An alternative approach to analyze lattice data for the vacuum polarization function is the method of *analytic continuation* [191] which is closely related to the work in refs. [192, 193].

The basic idea of this method is to express the hadronic vacuum polarization function through a spatial Fourier transformation and an exponential weight in time direction of the vector correlation function,

$$\bar{\Pi}(K^2)(K_\mu K_\nu - \delta_{\mu\nu} K^2) =$$
$$\int dt \, e^{\omega t} \int d^3\vec{x} \, e^{i\vec{k}\vec{x}} \langle \Omega | T\{J_\mu^E(\vec{x}, t) J_\nu^E(\vec{0}, 0)\} | \Omega \rangle \tag{46}$$

where $J_\mu^E(X)$ is the electromagnetic current, $K = (\vec{k}, -i\omega)$ with $\vec{k}$ the spatial momentum and ω the photon energy. The essential point is that only for the spatial indices a standard Fourier transformation is carried out while in time we have a real time transformation.

This method allows, in principle, to compute the HVP function at small space-like momenta and even at time-like momenta. We will show the feasibility of the method here at the example of the Adler function in fig. 19. Here we compare directly to a dispersive analysis [194]. As can be seen, although the errors of our lattice calculation is still larger, we find a very good agreement for the whole range of momenta, including time-like ones. In refs. [191, 195] the analytic continuation method has been employed for computing the leading order hadronic contribution of the muon anomalous magnetic moment. As a result it was found that

the analytic continuation method does lead to a similar accuracy as the standard method discussed above. It can thus, at least presently, be considered as an alternative approach to compute a_μ^{hvp}. It is worth stressing that the analytic continuation method is applicable for a much larger class of observables such as momentum dependent form factors and quantities related to scattering processes or resonances, see e.g. [196].
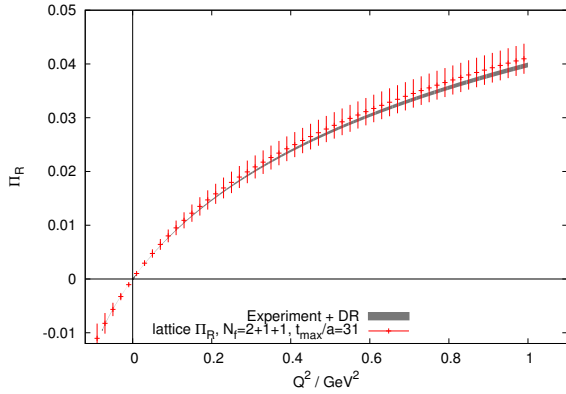

Figure 19: The renormalized vacuum polarization function from our lattice data ($a \approx 0.078\,\mathrm{fm}$, $V = (2.5\mathrm{fm})^3$) together with a comparison to the dispersion relation data from [194].

8.7. Charm quark mass and α_s

As a very interesting further application of the available vector correlators that has been used in the $N_f = 2+1+1$ computation of the hadronic contribution to the muon anomalous magnetic moment is their short distance behaviour for the charm sector. The charm quark is sufficiently heavy to allow for a perturbative treatment of these correlators at short distances [197, 198].

The perturbative expansion can then be compared to either experiment or to lattice results. To be more specific, such a comparison is done by looking at the temporal moments in the framework of the so-called current correlator method [199]. The temporal moments in lattice QCD have their equivalent counterparts in experiment. There they can be extracted from the (energy) moments of the hadronic $e^+e^- \to \gamma^* \to$ hadrons cross-section ratio R, see e.g. ref. [200]. In perturbative QCD the low-order derivatives of the polarization functions associated with the quark-bilinear current-current correlators can be computed most remarkably at the 4-loop level. Comparing lattice results of such moments to their experimental counterpart can provide a direct test of QCD. In addition, comparing the perturbative QCD

results of the temporal moments to lattice results provides access to determine the fundamental QCD parameters α_s and the charm quark mass.

In Ref. [199] it has been demonstrated that the moments of current-current correlation functions can indeed be used to match to perturbation theory and to extract the strong coupling constant and the charm quark mass. We will here give the example of the vector current correlation function [201] but emphasize that also other current-current correlation functions can and have been used which stabilizes the analysis and gives more precise results.

The starting point is the correlation function

$$C_{jj}^{av}(t) = \frac{1}{V_3} \sum_{\vec{x}} J_j^C(\vec{x}, t) J_j^C(\vec{0}, 0) \qquad (47)$$

where $J_j^C(\vec{x}, t)$ is the vector current already discussed above. The correlation function of eq. (47) can be used to construct the moments

$$
\begin{aligned}
\mathcal{M}_{\mathrm{L}}^n &= \frac{1}{n!} \left(\frac{d}{d\hat{K}^2} \right)^n \Pi(\hat{K}^2) \Big|_{\hat{K}=0} \\
&= \frac{a^{2n}}{3} \sum_{s=1}^{t_{max}/a} C(s, n) C_{jj}^{av}(t)
\end{aligned}
\qquad (48)
$$

with the coefficient function

$$C(s, n) = 2s\,(-1)^{n+1} \frac{(s+n)!}{(s-n-1)!\,(2n+2)!} \;. \qquad (49)$$

A direct comparison of the so established moments with their experimental counterparts is given in table 9. As can be seen for the first four moments a convincing agreement is found. Using moments evaluated on the lattice with maximally twisted mass fermions and adding also those from the other current-current correlation functions, such as the pseudo scalar current, we have determined the charm quark mass and the strong coupling constant α_s. This could be achieved by making use of the Mathematica package of ref. [202].

In fig. 20, we give the $1 - \sigma$ contour graph for both quantities as determined in the chiral and the continuum limit. Clearly, while the charm quark mass can be extracted rather precisely, the Strong coupling constant has a large error. Nevertheless, when using α_s as an input, an accurate value for the charm quark mass can be achieved. Note however that intrinsic uncertainties of the perturbative expansion, as discussed partly in [203], can add a non-negligible systematic error.

no.	$\mathcal{M}_c^n \cdot 10^{2+n}$	$\mathcal{M}_L^{n,N_f=2} \cdot 10^{2+n}$	$\mathcal{M}_L^{n,N_f=2+1+1} \cdot 10^{2+n}$
1	4.115 (59)	4.191 (63)	4.152 (94)
2	2.844 (51)	2.872 (54)	2.828 (73)
3	2.493 (51)	2.528 (54)	2.462 (70)
4	2.373 (51)	2.397 (57)	2.299 (71)

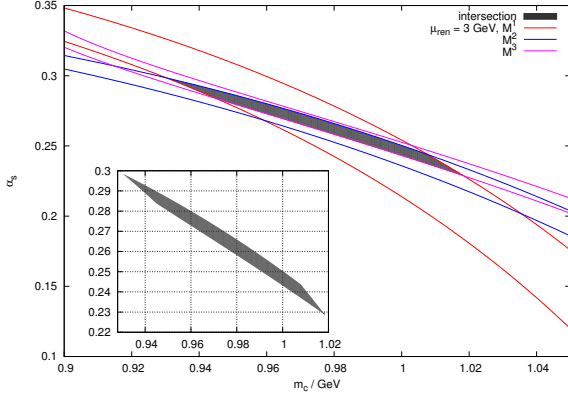Table 9: Comparison of continuum and lattice moments, given in units of GeV^{2n}, of order 1 to 4.

Figure 20: The 1-σ contour plot of the charm quark mass and α_s as extracted from temporal moments computed in our twisted mass lattice setup of QCD.

8.8. Other physical quantities

Within our work in the twisted mass lattice formulation of QCD, a number of other quantities have been computed that we here list shortly.

- Rather easy to access, but nevertheless important quantities are the meson decay constants f_K, f_D, f_{D_s}. In [204] we have performed a comprehensive analysis of these quantities for $N_f = 2$ mass-degenerate flavours of quarks. A first account for the setup of maximally twisted mass lattice QCD with $N_f = 2 + 1 + 1$ flavours of active sea quarks has been given in [205]. For the pseudo scalar decay constants we follow the mixed action approach described in section 7 by using so called Osterwalder-Seiler fermions in the valence sector for strange and charm quarks. The data for two values of the lattice spacing and several values of the up/down quark mass have been analyzed using chiral perturbation theory. In fig. 21 we show an example of such fits for the case of the pion and Kaon decay constants. Similar analyses have been performed for the the decay constants of the D- and the D_s mesons, f_D and f_{D_s}, using SU(2) heavy meson chiral perturbation theory [206], see also [204] and [204] for more details.
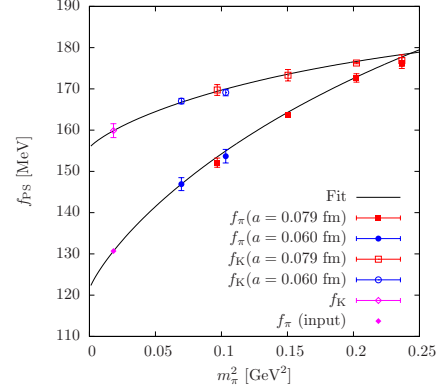

Figure 21: Pion and Kaon decay constants as a function of m_π^2. Data are shown for two values of the lattice spacing $a = 0.079$ fm and $a = 0.060$ fm.

N_f	f_K	f_D	f_{D_s}	V_{us}
2	158.1(2.4)	197(9)	244(8)	0.220(3)
2+1+1	160(2)	204(3)	248.9(5.3)	0.220(2)

Table 10: Our results for the pseudo scalar decay constants (in units of MeV) after extrapolation to the continuum and chiral limits. We also give our estimates for the CKM matrix element V_{us}. Values for both setups with $N_f = 2$ and $N_f = 2 + 1 + 1$ flavours are listed for which we take the values of f_K and V_{us} from ref. [205].

We mention that the result for f_K/f_π can give a value for the CKM matrix element V_{us}. To this end, the experimental measurement of $\Gamma(K \rightarrow \mu\bar{\nu}_\mu(\gamma))/\Gamma(\pi \rightarrow \mu\bar{\nu}_\mu(\gamma))$ [207] can be used to get first a determination of the ratio $|V_{us}|/|V_{ud}|$ [208]. Combing this with the determination $|V_{ud}| = 0.97425(22)$ [209] from nuclear beta decays, yields the estimate given in table 10.

- Another important quantity in QCD is the Λ parameter. We have determined $\Lambda_{\overline{MS}}$ for $n_f = 2$ dynamical quark flavours by fitting the $Q\bar{Q}$ static potential to perturbation theory [210]. There, the static potential is known analytically up to terms of $O(\alpha_s^4)$ and $\sim \alpha_s^4 \ln \alpha_s$ [211, 212]. The comparison of high-loop order of perturbation theory and lattice results of the static potential has become possible, due to recent advances in both perturbative calculations, namely the determination and publication of the last missing contribution to the $Q\bar{Q}$ static potential at $O(\alpha_s^4)$, and lattice simulations with $n_f = 2$ dynamical quark flavors performed at the rather fine lattice spacing of $a \approx 0.042$ fm.

We have undertaken a comprehensive analysis of

systematic effects [210] in the comparison with perturbation theory which leads to a value $\Lambda^{N_f=2}_{\overline{\text{MS}}} = 315(30)$ MeV where the error includes both the statistical and the systematic one. A similar analysis on the same twisted mass gluon field configurations, but performed in momentum space [213] yields a values of $\Lambda^{N_f=2}_{\overline{\text{MS}}} = 331(21)$ MeV which is fully compatible with our coordinate analysis of ref. [210].

- The Kaon bag parameter B_K controls $K^0 - \bar{K}^0$ oscillations. It is thus an important quantity and it is of fully non-perturbative nature, requiring a lattice QCD computation. We have calculated B_K in a partially quenched setup with two maximally twisted dynamical (sea) light Wilson quarks [214]. In the valence sector we used Osterwalder–Seiler fermions. Employing the non-perturbative RI-MOM scheme, in the continuum limit and at the physical value of the pion mass we get the renormalization group invariant quantity $B_K^{\text{RGI}} = 0.729 \pm 0.030$, see fig. 22.
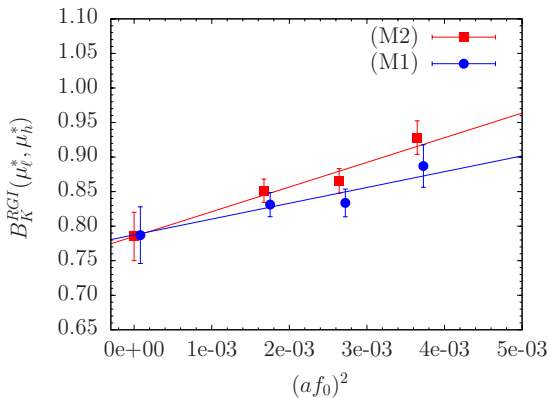

Figure 22: The renormalization group invariant Kaon bag parameter $B_{K,\text{lat}}^{\text{RGI}}$ as function of $(af_0)^2$, using two methods labeled as M1 and M2, which originate come from different procedures for evaluating the renormalization constants Z_{AV+VA} and Z_A. As can be seen in the graph $B_{K,\text{lat}}^{\text{RGI}}$ agrees in the continuum limit from the two methods used.

- Within this project, we have also developed a new method to extract B-physics parameters , e.g. the b-quark mass and decay constants [215]. The basic idea is to construct ratios of heavy-light meson masses and decay constants which assume an exactly known value in the static limit. By computing these ratios at various heavy quark masses covering the charm quark mass a smooth interpolation

–in contrast to the often used extrapolation– can be performed to the static limit. In this way, results for the b quark mass and various B-meson decay constant can be extracted and the systematic errors can be evaluated quantitatively. The method, first proposed in [215] has been very successfully applied for many quantities relevant for heavy flavour physics, see ref. [216] for a recent overview.

9. Conclusion and outlook

In this project of the transregional collaborative research center, we have established maximally twisted mass fermions as a valuable alternative for lattice QCD computations. In particular, we have demonstrated that this approach can be used to simulate the first two quark generations and to be able to reach the physical value of the pion mass.

Within the project a large number of physical quantities has been calculated spanning fundamental parameters of QCD, decay constants, scattering phenomena and hadronic contributions to electroweak observables. For the computations of these quantities, it has been instrumental that with twisted mass fermions at maximal twisted automatic $O(a)$-improvement can be realized. This led to small cutoff effects and allowed controlled continuum limit extrapolations in many cases without the need to compute further improvement coefficients.

Within the project discussed here also new directions emerged. The first is the extension of the simulations to the case of non-zero temperature, where the phase structure of twisted mass fermions [217] and the equation of state [218, 219, 220] could be determined. For this work, information from the results at zero temperature as described in this contribution has been very important to set the physical scale and to tune the non-zero temperature setup to maximal twist. Details of the non-zero temperature simulations are given in a separate contribution [81].

Another effort has been started within this project to revisit the Hamiltonian approach to lattice field theory. Employing the method of tensor network –and in particular matrix product– states, it has been demonstrated at the example of the Schwinger model that it is possible to compute the spectrum [221] of the model and also to address non-zero temperature [222]. These first very encouraging results could open the way to perform computations at a non-zero chemical potential and also perform real time simulations. Although this is clearly a fascinating perspective, it needs still new theoretical and conceptual developments to apply the tensor network technique to lattice QCD.

As a final development initiated in this project, we mention the Quasi Monte Carlo (QMC) technique which we used for the first time for a lattice model, the quantum mechanical harmonic and anharmonic oscillator [223, 224]. This approach can change the error behaviour of a standard Markov Chain Monte Carlo simulation from $1/\sqrt{N}$ to $1/N$ or even better with N the number of samples. Again, investigations of this approach are in their infancy and it is to be awaited, whether the QMC technique can be used for realistic quantum field theoretical models in higher dimensions.

In summary, the goal of this work has been the investigation of new approaches to address questions in lattice field theory with an emphasis on lattice QCD. The fact that we now are performing simulations at the physical point with new algorithmic techniques that were developed in this project shows that the project has been successful. It has also been very rewarding that further new methods could be developed, such as special techniques to compute dis-connected graphs, the extension to non-zero temperature and the first calculations with matrix product states and QMC.

References

[1] A. Abdel-Rehim *et al.*, PoS **LATTICE2013**, 264 (2013), `arXiv:1311.4522 [hep-lat]`.

[2] A. Abdel-Rehim *et al.*, PoS **LATTICE2014**, 119 (2014), `arXiv:1411.6842 [hep-lat]`.

[3] **Particle Data Group** Collaboration, K. Olive *et al.*, Chin.Phys. **C38**, 090001 (2014).

[4] F. Burger, G. Hotzel, K. Jansen and M. Petschlies, PoS **LATTICE2014**, 145 (2014), `arXiv:1411.0705 [hep-lat]`.

[5] A. De Freitas and J. Blümlein, this proceedings .

[6] H. Neuberger, Phys. Lett. **B417**, 141 (1998), `hep-lat/9707022`.

[7] H. Neuberger, Phys. Lett. **B427**, 353 (1998), `hep-lat/9801031`.

[8] M. Lüscher, Phys. Lett. **B428**, 342 (1998), `hep-lat/9802011`.

[9] T. Chiarappa *et al.*, `hep-lat/0409107`.

[10] T. Chiarappa *et al.*, `arXiv:hep-lat/0609023`.

[11] **ALPHA** Collaboration, R. Frezzotti, P. A. Grassi, S. Sint and P. Weisz, JHEP **08**, 058 (2001), `hep-lat/0101001`.

[12] R. Frezzotti and G. C. Rossi, JHEP **08**, 007 (2004), `hep-lat/0306014`.

[13] K. G. Wilson, Phys. Rev. **D10**, 2445 (1974).

[14] H. B. Nielsen and M. Ninomiya, Nucl. Phys. **B185**, 20 (1981).

[15] H. B. Nielsen and M. Ninomiya, Phys. Lett. **B105**, 219 (1981).

[16] D. Friedan, Commun.Math.Phys. **85**, 481 (1982).

[17] M. Bochicchio, L. Maiani, G. Martinelli, G. C. Rossi and M. Testa, Nucl.Phys. **B262**, 331 (1985).

[18] P. H. Ginsparg and K. G. Wilson, Phys. Rev. **D25**, 2649 (1982).

[19] F. Niedermayer, Nucl. Phys. Proc. Suppl. **73**, 105 (1999), `hep-lat/9810026`.

[20] P. Hasenfratz, V. Laliena and F. Niedermayer, Phys. Lett. **B427**, 125 (1998), `hep-lat/9801021`.

[21] P. Hasenfratz, Nucl. Phys. **B525**, 401 (1998), `hep-lat/9802007`.

[22] P. Hernandez, K. Jansen and M. Lüscher, Nucl. Phys. **B552**, 363 (1999), `hep-lat/9808010`.

[23] P. Hernandez, K. Jansen and L. Lellouch, Phys.Lett. **B469**, 198 (1999), `arXiv:hep-lat/9907022 [hep-lat]`.

[24] P. Hernandez, K. Jansen, L. Lellouch and H. Wittig, Nucl. Phys. Proc. Suppl. **106**, 766 (2002), `hep-lat/0110199`.

[25] P. Hernandez, K. Jansen, L. Lellouch and H. Wittig, JHEP **07**, 018 (2001), `hep-lat/0106011`.

[26] W. Bietenholz, K. Jansen and S. Shcheredin, JHEP **0307**, 033 (2003), `arXiv:hep-lat/0306022 [hep-lat]`.

[27] W. Bietenholz, T. Chiarappa, K. Jansen, K. Nagai and S. Shcheredin, JHEP **0402**, 023 (2004), `arXiv:hep-lat/0311012 [hep-lat]`.

[28] J. Osborn, D. Toublan and J. Verbaarschot, Nucl.Phys. **B540**, 317 (1999), `arXiv:hep-th/9806110 [hep-th]`.

[29] P. Damgaard, J. Osborn, D. Toublan and J. Verbaarschot, Nucl.Phys. **B547**, 305 (1999), `arXiv:hep-th/9811212 [hep-th]`.

[30] S. M. Nishigaki, P. H. Damgaard and T. Wettig, Phys.Rev. **D58**, 087704 (1998), `arXiv:hep-th/9803007 [hep-th]`.

[31] P. H. Damgaard and S. M. Nishigaki, Phys.Rev. **D63**, 045012 (2001), `arXiv:hep-th/0006111 [hep-th]`.

[32] G. Egri, Z. Fodor, S. Katz and K. Szabo, JHEP **0601**, 049 (2006), `arXiv:hep-lat/0510117 [hep-lat]`.

[33] P. Gerhold, `arXiv:1002.2569 [hep-lat]`.

[34] J. Bulava *et al.*, Adv.High Energy Phys. **2013**, 875612 (2013), `arXiv:1210.1798` [hep-lat].

[35] P. Gerhold and K. Jansen, JHEP **0709**, 041 (2007), `arXiv:0705.2539` [hep-lat].

[36] P. Gerhold and K. Jansen, JHEP **0710**, 001 (2007), `arXiv:0707.3849` [hep-lat].

[37] P. Gerhold and K. Jansen, JHEP **0907**, 025 (2009), `arXiv:0902.4135` [hep-lat].

[38] P. Gerhold and K. Jansen, JHEP **1004**, 094 (2010), `arXiv:1002.4336` [hep-lat].

[39] P. Gerhold, K. Jansen and J. Kallarackal, Phys.Lett. **B710**, 697 (2012), `arXiv:1111.4789` [hep-lat].

[40] P. Gerhold, K. Jansen and J. Kallarackal, JHEP **1101**, 143 (2011), `arXiv:1011.1648` [hep-lat].

[41] J. Bulava, K. Jansen and A. Nagy, Phys.Lett. **B723**, 95 (2013), `arXiv:1301.3416`.

[42] P. Hegde, K. Jansen, C.-J. D. Lin and A. Nagy, `arXiv:1310.6260` [hep-lat].

[43] A. Shindler, Phys. Rept. **461**, 37 (2008), `arXiv:0707.4093` [hep-lat].

[44] χ**LF** Collaboration, W. Bietenholz *et al.*, JHEP **12**, 044 (2004), `hep-lat/0411001`.

[45] χ_{L}**F** Collaboration, K. Jansen, A. Shindler, C. Urbach and I. Wetzorke, Phys. Lett. **B586**, 432 (2004), `hep-lat/0312013`.

[46] χ**LF** Collaboration, K. Jansen, M. Papinutto, A. Shindler, C. Urbach and I. Wetzorke, Phys. Lett. **B619**, 184 (2005), `hep-lat/0503031`.

[47] χ**LF** Collaboration, K. Jansen, M. Papinutto, A. Shindler, C. Urbach and I. Wetzorke, JHEP **09**, 071 (2005), `hep-lat/0507010`.

[48] **ETM** Collaboration, R. Baron *et al.*, JHEP **1008**, 097 (2010), `arXiv:0911.5061` [hep-lat].

[49] **ETM** Collaboration, C. Urbach, PoS **LAT2007**, 022 (2007), `arXiv:0710.1517` [hep-lat].

[50] **ETM Collaboration** Collaboration, P. Dimopoulos, R. Frezzotti, G. Herdoiza, C. Urbach and U. Wenger, PoS **LAT2007**, 102 (2007), `arXiv:0710.2498` [hep-lat].

[51] **European Twisted Mass Collaboration** Collaboration, C. Alexandrou *et al.*, Phys.Rev. **D78**, 014509 (2008), `arXiv:0803.3190` [hep-lat].

[52] R. Frezzotti, G. Martinelli, M. Papinutto and G. Rossi, JHEP **0604**, 038 (2006), `arXiv:hep-lat/0503034` [hep-lat].

[53] χ**LF** Collaboration, K. Jansen *et al.*, Phys. Lett. **B624**, 334 (2005), `hep-lat/0507032`.

[54] G. Colangelo, U. Wenger and J. M. Wu, Phys.Rev. **D82**, 034502 (2010), `arXiv:1003.0847` [hep-lat].

[55] S. Aoki and O. Bar, Eur.Phys.J. **A31**, 481 (2007), `arXiv:hep-lat/0610085` [hep-lat].

[56] O. Bar, Phys.Rev. **D82**, 094505 (2010), `arXiv:1008.0784` [hep-lat].

[57] **ETM** Collaboration, P. Dimopoulos, R. Frezzotti, C. Michael, G. Rossi and C. Urbach, Phys.Rev. **D81**, 034509 (2010), `arXiv:0908.0451` [hep-lat].

[58] **ETM** Collaboration, P. Boucaud *et al.*, Phys. Lett. **B650**, 304 (2007), `arXiv:hep-lat/0701012`.

[59] L. Del Debbio, L. Giusti, M. Luscher, R. Petronzio and N. Tantalo, JHEP **0702**, 056 (2007), `arXiv:hep-lat/0610059` [hep-lat].

[60] L. Del Debbio, L. Giusti, M. Luscher, R. Petronzio and N. Tantalo, JHEP **0702**, 082 (2007), `arXiv:hep-lat/0701009` [hep-lat].

[61] I. Montvay, Nucl.Phys. **B466**, 259 (1996), `arXiv:hep-lat/9510042` [hep-lat].

[62] C. Urbach, K. Jansen, A. Shindler and U. Wenger, Comput. Phys. Commun. **174**, 87 (2006), `hep-lat/0506011`.

[63] F. Bodin *et al.*, Comput.Phys.Commun. **147**, 402 (2002).

[64] F. Farchioni *et al.*, Eur. Phys. J. **C39**, 421 (2005), `hep-lat/0406039`.

[65] F. Farchioni *et al.*, Eur. Phys. J. **C42**, 73 (2005), `hep-lat/0410031`.

[66] F. Farchioni *et al.*, Phys. Lett. **B624**, 324 (2005), `hep-lat/0506025`.

[67] F. Farchioni *et al.*, Eur. Phys. J. **C47**, 453 (2006), `hep-lat/0512017`.

[68] S. R. Sharpe and J. Singleton, R., Phys. Rev. **D58**, 074501 (1998), `hep-lat/9804028`.

[69] S. Aoki, Phys.Rev. **D30**, 2653 (1984).

[70] S. R. Sharpe and J. M. S. Wu, Phys. Rev. **D71**, 074501 (2005), `hep-lat/0411021`.

[71] S. R. Sharpe and J. M. S. Wu, Phys. Rev. **D70**, 094029 (2004), `hep-lat/0407025`.

[72] G. Münster, JHEP **09**, 035 (2004), `hep-lat/0407006`.

[73] G. Münster and C. Schmidt, Europhys. Lett. **66**, 652 (2004), `hep-lat/0311032`.

[74] G. Münster and T. Sudmann, JHEP **1104**, 116 (2011), `arXiv:1103.1494` [hep-lat].

[75] S. Aoki and O. Bär, Phys. Rev. **D70**, 116011 (2004), `hep-lat/0409006`.

[76] S. Aoki and O. Bär, `hep-lat/0509002`.

[77] E.-M. Ilgenfritz, W. Kerler, M. Müller-Preussker, A. Sternbeck and H. Stüben, Phys.Rev. **D69**, 074511 (2004), `arXiv:hep-lat/0309057` [hep-lat].

[78] F. Farchioni *et al.*, Nucl. Phys. Proc. Suppl. **140**, 240 (2005), `hep-lat/0409098`.

[79] P. Weisz, Nucl. Phys. **B212**, 1 (1983).

[80] P. Weisz and R. Wohlert, Nucl. Phys. **B236**, 397 (1984).

[81] F. Burger and M. Müller-Preussker, this proceedings .

[82] S. Duane, A. D. Kennedy, B. J. Pendleton and D. Roweth, Phys. Lett. **B195**, 216 (1987).

[83] M. Hasenbusch, Phys. Lett. **B519**, 177 (2001), `hep-lat/0107019`.

[84] M. Hasenbusch and K. Jansen, Nucl. Phys. **B659**, 299 (2003).

[85] **CP-PACS and JLQCD** Collaboration, A. Ukawa, Nucl. Phys. Proc. Suppl. **106**, 195 (2002).

[86] K. Jansen, Nucl. Phys. Proc. Suppl. **129**, 3 (2004), `hep-lat/0311039`.

[87] K. Jansen and C. Urbach, Comput.Phys.Commun. **180**, 2717 (2009), `arXiv:0905.3331` [hep-lat].

[88] E. tmLQCD software package, `https://github.com/etmc/tmLQCD`.

[89] M. Lüscher, Comput. Phys. Commun. **165**, 199 (2005), `arXiv:hep-lat/0409106`.

[90] M. Lüscher, JHEP **12**, 011 (2007), `arXiv:0710.5417` [hep-lat].

[91] M. A. Clark and A. D. Kennedy, Phys. Rev. **D75**, 011502 (2007), `arXiv:hep-lat/0610047`.

[92] M. Luscher, `arXiv:1002.4232` [hep-lat].

[93] A. Abdel-Rehim *et al.*, `arXiv:1311.5495` [hep-lat].

[94] A. Deuzeman, K. Jansen, B. Kostrzewa and C. Urbach, PoS **LATTICE2013**, 416 (2013), `arXiv:1311.4521` [hep-lat].

[95] **ETM** Collaboration, P. Boucaud *et al.*, Comput.Phys.Commun. **179**, 695 (2008), `arXiv:0803.0224` [hep-lat].

[96] S. Weinberg, Physica **A96**, 327 (1979).

[97] J. Gasser and H. Leutwyler, Ann. Phys. **158**, 142 (1984).

[98] J. Gasser and H. Leutwyler, Nucl. Phys. **B250**, 465 (1985).

[99] G. Colangelo and S. Durr, Eur.Phys.J. **C33**, 543 (2004), `arXiv:hep-lat/0311023` [hep-lat].

[100] G. Colangelo, S. Dürr and C. Haefeli, Nucl. Phys. **B721**, 136 (2005), `hep-lat/0503014`.

[101] E. E. Scholz, PoS **LAT2009**, 005 (2009), `arXiv:0911.2191 [hep-lat]`.

[102] **Muon G-2 Collaboration** Collaboration, G. Bennett *et al.*, Phys. Rev. **D73**, 072003 (2006), `arXiv:hep-ex/0602035 [hep-ex]`.

[103] B. L. Roberts, Chin.Phys. **C34**, 741 (2010), `arXiv:1001.2898 [hep-ex]`.

[104] F. Jegerlehner and A. Nyffeler, Phys. Rept. **477**, 1 (2009), `arXiv:arXiv:0902.3360 [hep-ph]`.

[105] T. Blum, Phys. Rev. Lett. **91**, 052001 (2003), `arXiv:hep-lat/0212018`.

[106] X. Feng, K. Jansen, M. Petschlies and D. B. Renner, Phys.Rev.Lett. **107**, 081802 (2011), `arXiv:1103.4818 [hep-lat]`.

[107] F. Burger *et al.*, `arXiv:1308.4327 [hep-lat]`.

[108] C. Aubin, T. Blum, M. Golterman and S. Peris, Phys.Rev. **D86**, 054509 (2012), `arXiv:1205.3695 [hep-lat]`.

[109] X. Feng, K. Jansen and D. B. Renner, Phys.Rev. **D83**, 094505 (2011), `arXiv:1011.5288 [hep-lat]`.

[110] D. B. Renner, X. Feng, K. Jansen and M. Petschlies, PoS **LATTICE2011**, 022 (2012), `arXiv:1206.3113 [hep-lat]`.

[111] M. Luscher, Commun. Math. Phys. **104**, 177 (1986).

[112] M. Luscher, Commun. Math. Phys. **105**, 153 (1986).

[113] M. Luscher, Nucl. Phys. **B354**, 531 (1991).

[114] X. Feng, K. Jansen and D. B. Renner, Phys.Lett. **B684**, 268 (2010), `arXiv:0909.3255 [hep-lat]`.

[115] M. I. Buchoff, J.-W. Chen and A. Walker-Loud, Phys.Rev. **D79**, 074503 (2009), `arXiv:0810.2464 [hep-lat]`.

[116] **NPLQCD** Collaboration, S. R. Beane, P. F. Bedaque, K. Orginos and M. J. Savage, Phys. Rev. **D73**, 054503 (2006), `arXiv:hep-lat/0506013`.

[117] S. R. Beane *et al.*, Phys. Rev. **D77**, 014505 (2008), `arXiv:0706.3026 [hep-lat]`.

[118] **CP-PACS** Collaboration, T. Yamazaki *et al.*, Phys. Rev. **D70**, 074-513 (2004), `arXiv:hep-lat/0402025`.

[119] G. Colangelo, J. Gasser and H. Leutwyler, Phys. Lett. **B488**, 261 (2000), `arXiv:hep-ph/0007112`.

[120] D. Djukanovic, J. Gegelia, A. Keller and S. Scherer, Phys. Lett. **B680**, 235 (2009), `arXiv:0902.4347 [hep-ph]`.

[121] D. Djukanovic, J. Gegelia, A. Keller and S. Scherer, `arXiv:1001.1772 [hep-ph]`.

[122] J. J. Dudek, R. G. Edwards and C. E. Thomas, Phys.Rev. **D87**, 034505 (2013), `arXiv:1212.0830 [hep-ph]`.

[123] C. Thomas, PoS **LATTICE2013**, 003 (2013).

[124] **ETM Collaboration** Collaboration, M. Constantinou *et al.*, JHEP **1008**, 068 (2010), `arXiv:1004.1115 [hep-lat]`.

[125] C. Alexandrou, M. Constantinou, T. Korzec, H. Panagopoulos and F. Stylianou, Phys.Rev. **D83**, 014503 (2011), `arXiv:1006.1920 [hep-lat]`.

[126] C. Alexandrou, M. Constantinou, T. Korzec, H. Panagopoulos and F. Stylianou, Phys.Rev. **D86**, 014505 (2012), `arXiv:1201.5025 [hep-lat]`.

[127] **ETM Collaboration** Collaboration, B. Blossier *et al.*, PoS **LATTICE2011**, 233 (2011), `arXiv:1112.1540 [hep-lat]`.

[128] G. Martinelli, C. Pittori, C. T. Sachrajda, M. Testa and A. Vladikas, Nucl. Phys. **B445**, 81 (1995), `arXiv:hep-lat/9411010`.

[129] M. Constantinou *et al.*, Phys.Rev. **D87**, 096019 (2013), `arXiv:1303.6776 [hep-lat]`.

[130] K. Chetyrkin and A. Retey, Nucl.Phys. **B583**, 3 (2000), `arXiv:hep-ph/9910332 [hep-ph]`.

[131] J. Gracey, Nucl.Phys. **B667**, 242 (2003), `arXiv:hep-ph/0306163 [hep-ph]`.

[132] J. Gracey, Nucl.Phys. **B662**, 247 (2003), `arXiv:hep-ph/0304113 [hep-ph]`.

[133] J. G. Lopez, K. Jansen, D. Renner and A. Shindler, Nucl.Phys. **B867**, 609 (2013), `arXiv:1208.4661 [hep-lat]`.

[134] J. G. Lopez, K. Jansen, D. Renner and A. Shindler, Nucl.Phys. **B867**, 567 (2013), `arXiv:1208.4591 [hep-lat]`.

[135] M. Luscher, R. Narayanan, P. Weisz and U. Wolff, Nucl.Phys. **B384**, 168 (1992), `arXiv:hep-lat/9207009 [hep-lat]`.

[136] S. Sint and R. Sommer, Nucl.Phys. **B465**, 71 (1996), `arXiv:hep-lat/9508012 [hep-lat]`.

[137] K. Jansen *et al.*, Phys.Lett. **B372**, 275 (1996), `arXiv:hep-lat/9512009 [hep-lat]`.

[138] S. Sint, Nucl.Phys. **B847**, 491 (2011), `arXiv:1008.4857 [hep-lat]`.

[139] V. Gimenez *et al.*, Phys.Lett. **B598**, 227 (2004), `arXiv:hep-lat/0406019 [hep-lat]`.

[140] K. Cichy, K. Jansen and P. Korcyl, Nucl.Phys. **B865**, 268 (2012), `arXiv:1207.0628 [hep-lat]`.

[141] T. Chiarappa *et al.*, Eur.Phys.J. **C50**, 373 (2007), `arXiv:hep-lat/0606011 [hep-lat]`.

[142] ETM Collaboration, R. Baron *et al.*, JHEP **1006**, 111 (2010), `arXiv:1004.5284 [hep-lat]`.

[143] **European Twisted Mass Collaboration** Collaboration, R. Baron *et al.*, Comput.Phys.Commun. **182**, 299 (2011), `arXiv:1005.2042 [hep-lat]`.

[144] G. Herdoiza, PoS **LATTICE2010**, 010 (2010), `arXiv:1103.1523 [hep-lat]`.

[145] R. Frezzotti and G. C. Rossi, Nucl. Phys. Proc. Suppl. **128**, 193 (2004), `hep-lat/0311008`.

[146] R. Frezzotti and G. C. Rossi, JHEP **10**, 070 (2004), `hep-lat/0407002`.

[147] K. Osterwalder and E. Seiler, Ann. Phys. **110**, 440 (1978).

[148] **ETM Collaboration** Collaboration, C. Alexandrou *et al.*, Phys.Rev. **D80**, 114503 (2009), `arXiv:0910.2419 [hep-lat]`.

[149] C. Alexandrou, V. Drach, K. Jansen, C. Kallidonis and G. Koutsou, `arXiv:1406.4310 [hep-lat]`.

[150] **Particle Data Group** Collaboration, K. Hagiwara *et al.*, Phys.Rev. **D66**, 010001 (2002).

[151] **BMW** Collaboration, S. Dürr *et al.*, Science **322**, 1224 (2008), `arXiv:0906.3599 [hep-lat]`.

[152] **PACS-CS** Collaboration, S. Aoki *et al.*, `arXiv:0807.1661 [hep-lat]`.

[153] T. Banks and A. Casher, Nucl.Phys. **B169**, 103 (1980).

[154] L. Giusti and M. Luscher, JHEP **0903**, 013 (2009), `arXiv:0812.3638 [hep-lat]`.

[155] L. Giusti, G. Rossi and M. Testa, Phys.Lett. **B587**, 157 (2004), `arXiv:hep-lat/0402027 [hep-lat]`.

[156] M. Luscher, Phys.Lett. **B593**, 296 (2004), `arXiv:hep-th/0404034 [hep-th]`.

[157] M. Luscher and F. Palombi, JHEP **1009**, 110 (2010), `arXiv:1008.0732 [hep-lat]`.

[158] K. Cichy, E. Garcia-Ramos and K. Jansen, JHEP **1310**, 175 (2013), `arXiv:1303.1954 [hep-lat]`.

[159] K. Cichy, E. Garcia-Ramos, K. Jansen and A. Shindler, PoS **LATTICE2013**, 129 (2013), `arXiv:1312.3535 [hep-lat]`.

[160] K. Cichy, E. Garcia-Ramos, K. Jansen and A. Shindler, PoS **LATTICE2013**, 128 (2013), `arXiv:1312.3534 [hep-lat]`.

[161] R. Sommer, PoS **LATTICE2013**, 015 (2014), `arXiv:1401.3270 [hep-lat]`.

[162] G. P. Engel, L. Giusti, S. Lottini and R. Sommer, `arXiv:1406.4987 [hep-ph]`.

[163] **RBC-UKQCD** Collaboration, Y. Aoki *et al.*, Phys.Rev. **D83**, 074508 (2011), `arXiv:1011.0892 [hep-lat]`.

[164] A. Bazavov *et al.*, Rev.Mod.Phys. **82**, 1349 (2010), `arXiv:0903.3598 [hep-lat]`.

[165] A. Bazavov *et al.*, PoS **LATTICE2010**, 083 (2010), `arXiv:1011.1792 [hep-lat]`.

[166] S. Borsanyi *et al.*, Phys.Rev. **D88**, 014513 (2013), `arXiv:1205.0788 [hep-lat]`.

[167] **ETMC** Collaboration, B. Blossier *et al.*, Phys.Rev. **D82**, 114513 (2010), `arXiv:1010.3659 [hep-lat]`.

[168] C. McNeile *et al.*, Phys.Rev. **D87**, 034503 (2013), `arXiv:1211.6577 [hep-lat]`.

[169] F. Burger, V. Lubicz, M. Mller-Preussker, S. Simula and C. Urbach, Phys.Rev. **D87**, 034514 (2013), `arXiv:1210.0838 [hep-lat]`.

[170] P. Hasenfratz and H. Leutwyler, Nucl.Phys. **B343**, 241 (1990).

[171] F. Hansen, Nucl.Phys. **B345**, 685 (1990).

[172] K. Jansen, A. Nube and A. Shindler, PoS **LATTICE2008**, 083 (2008), `arXiv:0810.0300 [hep-lat]`.

[173] G. Akemann, P. Damgaard, K. Splittorff and J. Verbaarschot, Phys.Rev. **D83**, 085014 (2011), `arXiv:1012.0752 [hep-lat]`.

[174] K. Splittorff and J. Verbaarschot, Phys.Rev. **D85**, 105008 (2012), `arXiv:1201.1361 [hep-lat]`.

[175] L. Giusti, M. Luscher, P. Weisz and H. Wittig, JHEP **0311**, 023 (2003), `arXiv:hep-lat/0309189 [hep-lat]`.

[176] **ETM** Collaboration, K. Cichy, E. Garcia-Ramos and K. Jansen, JHEP **1402**, 119 (2014), `arXiv:1312.5161 [hep-lat]`.

[177] **ALPHA Collaboration** Collaboration, S. Schaefer, R. Sommer and F. Virotta, Nucl.Phys. **B845**, 93 (2011), `arXiv:1009.5228 [hep-lat]`.

[178] E. Witten, Nucl.Phys. **B156**, 269 (1979).

[179] G. Veneziano, Nucl.Phys. **B159**, 213 (1979).

[180] L. Giusti, G. Rossi, M. Testa and G. Veneziano, Nucl.Phys. **B628**, 234 (2002), `arXiv:hep-lat/0108009 [hep-lat]`.

[181] **ETM** Collaboration, K. Jansen, C. Michael and C. Urbach, Eur.Phys.J. **C58**, 261 (2008), `arXiv:0804.3871 [hep-lat]`.

[182] **ETM collaboration** Collaboration, K. Ottnad *et al.*, JHEP **1211**, 048 (2012), `arXiv:1206.6719 [hep-lat]`.

[183] **ETM Collaboration** Collaboration, C. Michael, K. Ottnad and C. Urbach, Phys.Rev.Lett. **111**, 181602 (2013), `arXiv:1310.1207 [hep-lat]`.

[184] B. Chakraborty *et al.*, `arXiv:1403.1778 [hep-lat]`.

[185] T. Blum, T. Izubuchi and E. Shintani, Phys.Rev. **D88**, 094503 (2013), `arXiv:1208.4349 [hep-lat]`.

[186] E. Shintani *et al.*, `arXiv:1402.0244 [hep-lat]`.

[187] M. Davier, A. Hoecker, B. Malaescu and Z. Zhang, Eur. Phys. J. **C71**, 1515 (2011), `arXiv:1010.4180 [hep-ph]`.

[188] F. Jegerlehner and R. Szafron, Eur.Phys.J. **C71**, 1632 (2011), `arXiv:1101.2872 [hep-ph]`.

[189] K. Hagiwara, R. Liao, A. D. Martin, D. Nomura and T. Teubner, J.Phys. **G38**, 085003 (2011), `arXiv:1105.3149 [hep-ph]`.

[190] M. Benayoun *et al.*, Eur.Phys.J. **C73**, 2453 (2013), `arXiv:1210.7184 [hep-ph]`.

[191] X. Feng *et al.*, Phys.Rev. **D88**, 034505 (2013), `arXiv:1305.5878 [hep-lat]`.

[192] X.-d. Ji and C.-w. Jung, Phys.Rev.Lett. **86**, 208 (2001), `arXiv:hep-lat/0101014 [hep-lat]`.

[193] H. B. Meyer, Phys.Rev.Lett. **107**, 072002 (2011), `arXiv:1105.1892 [hep-lat]`.

[194] F. Jegerlehner, Nuovo Cim. **C034S1**, 31 (2011), `arXiv:1107.4683 [hep-ph]`.

[195] X. Feng *et al.*, `arXiv:1311.0652 [hep-lat]`.

[196] C. Alexandrou, M. Constantinou, G. Koutsou, K. Ottnad and M. Petschlies, `arXiv:1410.8818 [hep-lat]`.

[197] J. H. Kuhn, M. Steinhauser and C. Sturm, Nucl.Phys. **B778**, 192 (2007), `arXiv:hep-ph/0702103 [HEP-PH]`.

[198] K. Chetyrkin *et al.*, Phys.Rev. **D80**, 074010 (2009), `arXiv:0907.2110 [hep-ph]`.

[199] **HPQCD Collaboration** Collaboration, I. Allison *et al.*, Phys.Rev. **D78**, 054513 (2008), `arXiv:0805.2999 [hep-lat]`.

[200] J. H. Kuhn and M. Steinhauser, Nucl.Phys. **B619**, 588 (2001), `arXiv:hep-ph/0109084 [hep-ph]`.

[201] K. Jansen, M. Petschlies and C. Urbach, PoS **LATTICE2011**, 234 (2011), `arXiv:1111.5252 [hep-lat]`.

[202] K. Chetyrkin, J. H. Kuhn and M. Steinhauser, Comput.Phys.Commun. **133**, 43 (2000), `arXiv:hep-ph/0004189 [hep-ph]`.

[203] B. Dehnadi, A. H. Hoang, V. Mateu and S. M. Zebarjad, JHEP **1309**, 103 (2013), `arXiv:1102.2264 [hep-ph]`.

[204] **ETM Collaboration** Collaboration, B. Blossier *et al.*, JHEP **0907**, 043 (2009), `arXiv:0904.0954 [hep-lat]`.

[205] F. Farchioni *et al.*, PoS **LATTICE2010**, 128 (2010), `arXiv:1012.0200 [hep-lat]`.

[206] S. R. Sharpe and Y. Zhang, Phys.Rev. **D53**, 5125 (1996), `arXiv:hep-lat/9510037 [hep-lat]`.

[207] **FlaviaNet Working Group on Kaon Decays** Collaboration, M. Antonelli *et al.*, `arXiv:0801.1817 [hep-ph]`.

[208] W. J. Marciano, Phys.Rev.Lett. **93**, 231803 (2004), `arXiv:hep-ph/0402299 [hep-ph]`.

[209] J. Hardy and I. Towner, Phys.Rev. **C79**, 055502 (2009), `arXiv:0812.1202 [nucl-ex]`.

[210] **ETM Collaboration** Collaboration, K. Jansen, F. Karbstein, A. Nagy and M. Wagner, JHEP **1201**, 025 (2012), `arXiv:1110.6859 [hep-ph]`.

[211] A. V. Smirnov, V. A. Smirnov and M. Steinhauser, Phys.Rev.Lett. **104**, 112002 (2010), `arXiv:0911.4742 [hep-ph]`.

[212] C. Anzai, Y. Kiyo and Y. Sumino, Phys.Rev.Lett. **104**, 112003 (2010), `arXiv:0911.4335 [hep-ph]`.

[213] F. Karbstein, A. Peters and M. Wagner, JHEP **1409**, 114 (2014), `arXiv:1407.7503 [hep-ph]`.

[214] **ETM Collaboration** Collaboration, M. Constantinou *et al.*, Phys.Rev. **D83**, 014505 (2011), `arXiv:1009.5606 [hep-lat]`.

[215] **ETM Collaboration** Collaboration, B. Blossier *et al.*, JHEP **1004**, 049 (2010), `arXiv:0909.3187 [hep-lat]`.

[216] **the ETM Collaboration** Collaboration, N. Carrasco *et al.*, `arXiv:1310.1851 [hep-lat]`.

[217] E.-M. Ilgenfritz *et al.*, Phys.Rev. **D80**, 094502 (2009), `arXiv:0905.3112 [hep-lat]`.

[218] **tmfT** Collaboration, F. Burger *et al.*, Phys.Rev. **D87**, 074508 (2013), `arXiv:1102.4530 [hep-lat]`.

[219] F. Burger, G. Hotzel, M. Mueller-Preussker, E. Ilgenfritz and M. Lombardo, PoS **LATTICE2013**, 153 (2014).

[220] F. Burger, E.-M. Ilgenfritz, M. P. Lombardo and M. Müller-Preussker, `arXiv:1412.6748 [hep-lat]`.

[221] M. Bauls, K. Cichy, K. Jansen and J. Cirac, JHEP **1311**, 158 (2013), `arXiv:1305.3765 [hep-lat]`.

[222] M. C. Bauls, K. Cichy, J. I. Cirac, K. Jansen and H. Saito, PoS **LATTICE2013**, 332 (2013), `arXiv:1310.4118 [hep-lat]`.

[223] A. Ammon *et al.*, `arXiv:1311.4726 [hep-lat]`.

[224] K. Jansen *et al.*, Comput.Phys.Commun. **185**, 948 (2014), `arXiv:1302.6419 [hep-lat]`.